MASTER THESIS

TITLE: Transport protocols performance on Visible Light Communication technology

MASTER's DEGREE: Master's degree in Applied Telecommunications and Engineering Management

AUTHOR: Federico Vincenzo Fiordigigli

ADVISORS: Cristina Cervelló Pastor, Sebastià Sallent Ribes

DATE: May, 8th 2018

Title: Transport protocols performance on Visible Light Communication technology

Author: Federico Vincenzo Fiordigigli

Advisors: Cristina Cervelló Pastor, Sebastià Sallent Ribes

Date: May, 8th 2018

Abstract

In the last decade, wireless communications have seen a dramatic growth of the traffic demand and the radio spectrum seems to not be able to keep this pace alone due to the limited available bandwidth. For this reason, Visible Light Communication is being considered as a potential access option for the next-generation of wireless communication technologies (5G) and it is gaining an increasing attention: this technology, which works modulating the intensity of the light in the "visible" part of the EM spectrum, use LEDs for the dual-purpose of illumination and communication. VLC shows great features such as ultra-high bandwidth, robustness to electromagnetic interference, a virtually unlimited frequency reuse and a cost effectiveness due to the unregulated spectrum and the use of the LEDs.

The aim of this work is to further analyze the performance of the TCP protocol in the VLC networks and to provide a tool for the simulation of complex VLC networks. Using the NS3 framework, an existing module has been further developed and tested to simulate a VLC network and a simple scenario, with an AP and a user moving in random walk on the boundaries. The TCP performance has been evaluated, comparing two congestion control algorithms (New Reno and Westwood) and analyzing different parameters such as throughput, dropped packets, congestion window behavior and end-to-end delay. After that, a new module has been designed and developed to overcome the limitations of the previous one, such as the two devices per channel limit and the inadequate interference model, and to allow more complex simulation scenarios.

The results obtained demonstrated the good qualities of the VLC channel, where the main limitations are due to the physical devices parameters, like the FOV and the semi-angle at half-power, that strictly define the coverage area. About the TCP performance analysis, the results showed that TCP works very well in the coverage, it has several problems handling the movement of the receiver among the boundaries. However, by analyzing different parameters such as the sender buffer size, the channel delay and the source application data rate, Westwood showed to have a better performance than New Reno, especially in terms of mean delay and BER**.**

CONTENTS

INTRODUCTION

5G, the next evolution of mobile broadband network, will bring new unique network and service capabilities: it will provide an order of magnitude improvement in performance in the areas of more capacity, lower latency, more mobility, more accuracy of terminal location, increased reliability and availability. In addition, it will allow the connection of many more devices simultaneously (Internet-of-Things) and to improve the terminal battery capacity life [1].

Visible Light Communication (VLC) is considered as a potential access option for 5G wireless communications and it is gaining an increasing attention in the last years [2]. VLC is a technology which takes full advantage of visible Light-Emitting Diodes (LEDs) for the dual purpose of illumination and data communications at very high speeds. VLC is a sustainable and green technology with the potential to revolutionize approaches to how we will use lights in the near future. It can provide solutions for several applications including wireless local area, personal area, and body area networks (WLAN, WPAN, and WBANs), heterogeneous networks, indoor localization and navigation (where current GPS is not available), vehicular networks, underground and underwater networks among others, offering a range of data rates from a few Mbps to 100 Gbps [3]. LiFi is a subset of VLC that exhibits high-speed, bidirectional, fully networked communications.

Most of the research work has focused on physical and MAC layer performance enhancements [4], but there has been a low interest in research for the network and transport layer. For this reason, this work aims to deepen the research in these fields providing the tools for better emulating the VLC and LiFi systems in one of the most used open source network simulators, ns-3 [5]. Furthermore, the behavior of TCP will be analyzed by simulating some scenarios with these tools.

The work is divided into six chapters including this initial introduction. Chapter 1 introduces an overview of VLC technology, with a detailed explanation of the channel model. Chapter 2 presents a theoretical background of the main concepts regarding TCP principles and TCP congestion control mechanisms. Chapter 3 contains an overview of the ns-3 simulator together with the design and the main characteristics of the modules implemented to emulate VLC technology. It also includes a summary of the simulation scenarios that were used for the analysis. Chapter 4 collects all the results obtained from the execution and data collection of the simulation scenarios. Several charts are presented along with the analysis of the results. Finally, the last chapter contains the conclusions of the research with some indication for the possible future work.

CHAPTER 1. VISIBLE LIGHT COMMUNICATION

In this chapter, the main aspects of VLC technology will be introduced, including the system architecture, the channel model, and the modulation schemes. In addition, the advantages and the challenges introduced are discussed.

1.1 VLC principles and LiFi

In the last decade, we have seen a dramatic increase in the traffic carried by the telecommunication networks, with the mobile traffic representing one of the main contributor: the last forecasts indicate that the total mobile data traffic is expected to rise at a compound annual growth rate of 42% and the monthly global traffic will surpass 100EB in 2023 [6].

These numbers are mainly due to the desire of human beings to communicate from anywhere at any time, and it has been satisfied by the Wireless technologies:
Wireless devices, applications and services have become very pervasive in our life, changing it radically.

Therefore, in order to keep the pace with this growing demand, it has been defined a new set of standards for the wireless and wire communications, the 5G (fifth generation) [7].

With the term Wireless communication, we usually refer to technologies that use radio waves to transfer information between two or more points without using a “wire” (electrical conductor). In fact, the Radio Frequency (RF) band, that lies between 30 kHz and 300 GHz of the Electromagnetic (EM) spectrum, has been the most used portion for communication purposes, mainly due to little interference in the frequency band and wide area coverage. However, the RF is just a part of the EM spectrum, as shown in Fig. 1.1.

We can see that it includes Infrared (IR), Visible and Ultraviolet (UV) light and these wavelengths are used in the so called Optical wireless communications (OWC) as unguided lights carrying a signal.

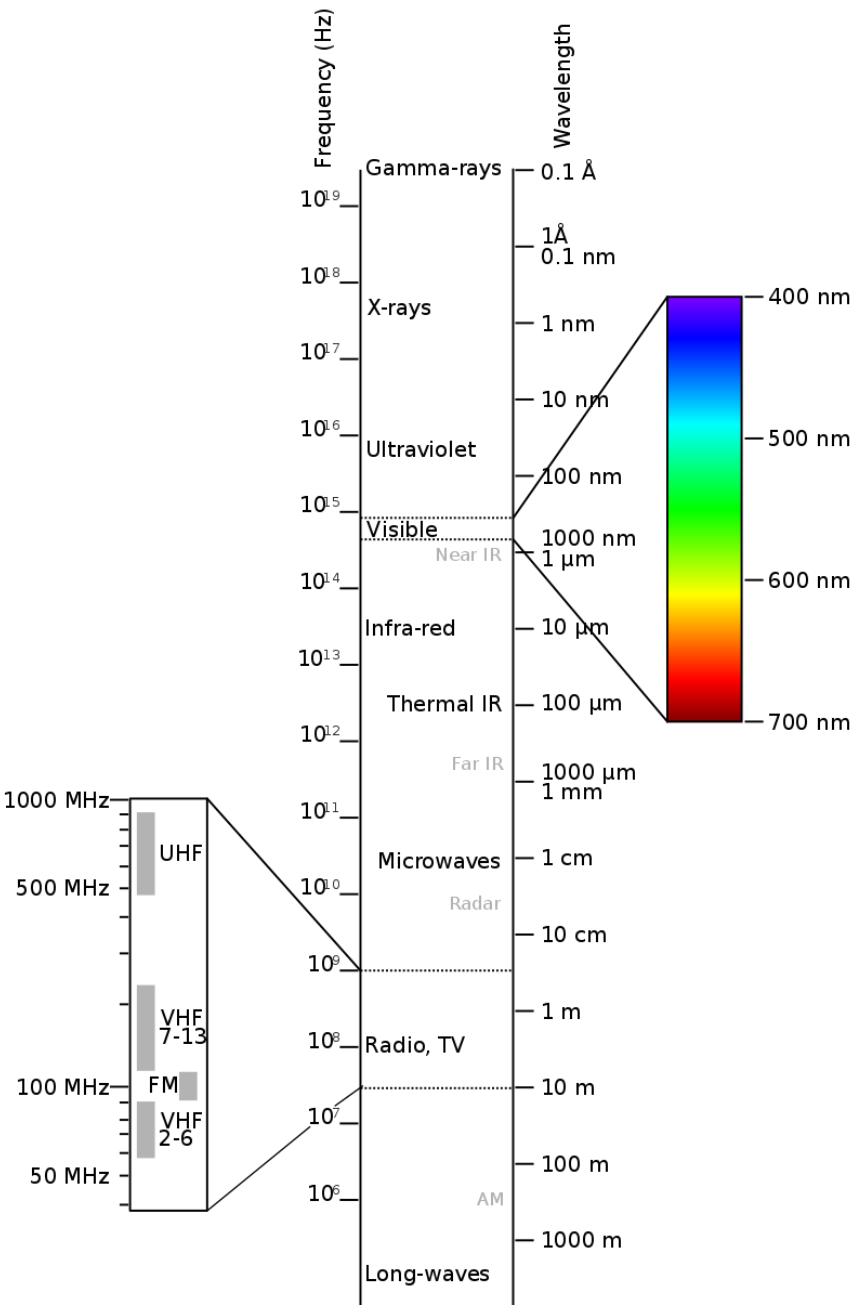

Fig. 1.1 The Electromagnetic spectrum (source Wikipedia)

OWC is a complementary technology to RF and it offers opportunities that are still mostly unexploited so far. In comparison to the RF counterparts. OWC shows greater features such as ultra-high bandwidth (in order of THz), robustness to electromagnetic interference, a high degree of spatial confinement bringing virtually unlimited frequency (or wavelength) reuse, and inherent physical security. In addition, since OWC technologies can operate in the unregulated spectrum, it provides cost effectiveness for several applications because no licensing fee is required [8].

When an OWC system uses the wavelengths from 390 to 700 nm (Fig. 1.1), we refer to it as Visible Light Communication (VLC): The peculiarity of this part of the

electromagnetic spectrum is to have waves with the ability of activate photoreceptor in the human cornea.

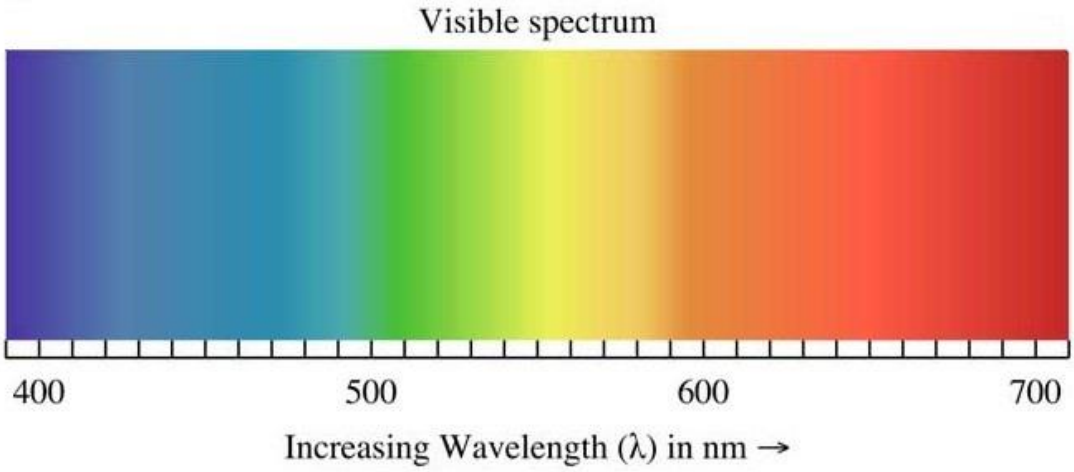

Fig. 1.2 EM spectrum visible to human eye (source Wikipedia)

VLC exploits solid-state lighting such as LEDs for data communication, modulating and transmitting a data stream by varying the intensity of luminaires. In other words, an LED can serve as a dual-purpose device, offering lighting and communication simultaneously, providing a viable solution to alleviating the spectrum shortage in the RF band [9].

There are several benefits to implementing VLC, among which [10]:

- VLC systems facilitate simple co-channel interference management and offer a high level of communication security. In indoor scenarios, the signals from VLC systems are confined by the walls of rooms, preventing interference by VLC systems in other rooms and potential eavesdropping.
- VLC is energy-efficient. Traditional indoor lighting or illumination is ubiquitous in the modern world and accounts for approximately 7% of the total electricity consumption in the USA [11]. Since in the last years the environment health and safety has become an important topic, governments around the world are encouraging the replacement of energy-inefficient halogen lamps and incandescent lamps with energy-efficient LEDs. This trend is paving the way for the development of ubiquitous VLC systems as LED illumination begins to spread widely. Furthermore, the energy used for communication in VLC is essentially free, as lighting is required anyway.

VLC not only has the potential to offer higher data rates but also has various important applications in the IoT, intelligent transportation systems, indoor positioning, and entertainment.

For the realization of truly mobile communication systems, a complete networking solution is required, which leads to the concept of Light-Fidelity (LiFi), antilogous to Wi-Fi. LiFi is a subset of VLC that exhibits high-speed, bidirectional, fully networked communications. The term was introduced the first time by Professor Harald Haas in [12]. For instance, in order to achieve communication with multiple VLC receivers in an indoor environment, a cellular network structure composed of several small optical attocells has been proposed [13].The goal is to provide seamless coverage and high spectral efficiency to multiple users simultaneously. In practice, an optical attocell network can be realized by installing multiple LiFi access points in the ceiling of a room.

The VLC system architecture, together with the channel model and the modulation schemes will be now introduced.

1.2 VLC system

The general communication link of a VLC system is shown in Fig. 1.3. [14]

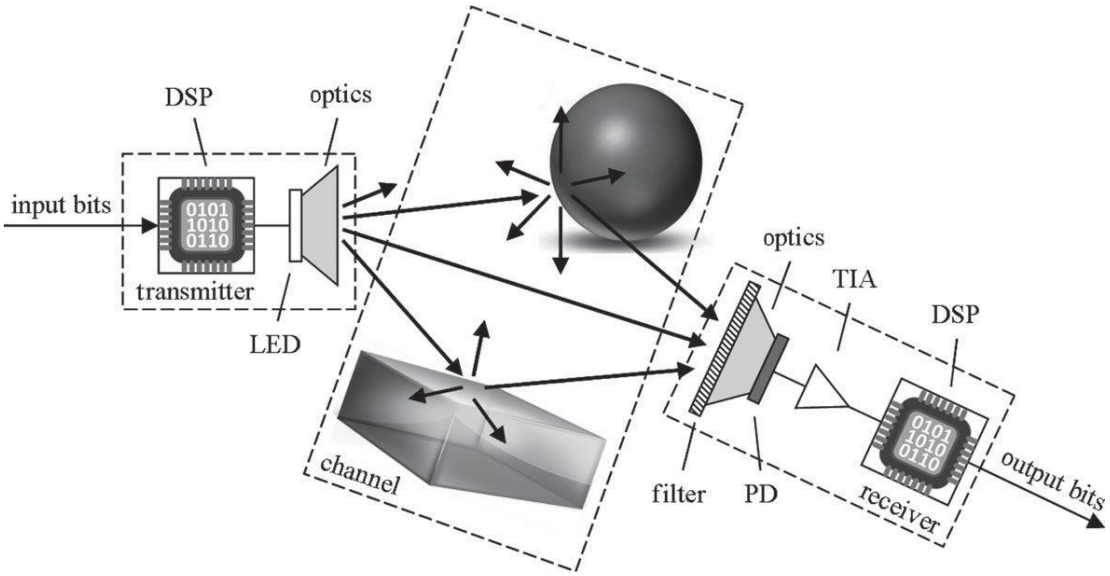

Fig. 1.3 Transmission link in VLC. The optical wireless channel includes several light rays and the reflecting objects [14]

The main components of the system are the transmitter (lighting source), the optical wireless channel and the receiver (the photodetector).

More in the details, the transmitter consists of a Digital Signal Processor (DSP) with a Digital-to-Analog Converter (DAC), which supply for the modulation of the digital information bits and their transformation into an analog current signal. This current signal, that carries the information, drives the optical emitter (i.e. an LED or an array of LEDs) and it is transformed into optical intensity.

The optical signal can be passed through an optical system to further shape the transmitted beam. Here, an optical amplifier lens, a collimator, or a diffusor can be employed to concentrate or broaden the beam.

The optical signal is then transmitted over the optical wireless channel. A portion of the optical energy is absorbed by the objects in the environment, and the rest is reflected back in a diffuse or specular manner.

Directed and reflected signal components arrive at the receiver. An optical filter is applied to reduce the interference from ambient light and, optionally, to select a portion of interest in the optical spectrum. Thereafter, the optical signal is passed through a system of optical elements (e.g. collimator lenses) to amplify the signal and to align the impinging light for optimum detection. At the photodetector (one PD or an array of PDs), the optical signal is converted back to electrical current.

The current signal is electronically pre-amplified by means of a transimpedance amplifier (TIA). A DSP with an analog-to-digital converter (ADC) is employed for transformation of the analog current signal into a digital signal and demodulation of the information bits.

1.3 Channel model

Before to introduce the channel model, it is necessary to introduce the possible link configurations, shown in Fig. 1.4. In [15] the authors defined two main criteria to classify them.

The first criterion is the degree of directionality of the transmitter and receiver. Directed links employ directional transmitters and receivers, which must be aimed in order to establish a link, while non-directed links employ wide-angle transmitters and receivers, alleviating the need for such pointing. Directed link design maximizes power efficiency, since it minimizes path loss and reception of ambient light noise. On the other hand, non-directed links may be more convenient to use, particularly for mobile terminals, since they do not require aiming of the transmitter or receiver. It is also possible to establish hybrid links, which combine transmitters and receivers having different degrees of directionality.

The second classification criterion relates to whether the link relies upon the existence of an uninterrupted Line-Of-Sight (LOS) path between the transmitter and receiver. LOS links rely upon such a path, while Non-Line-Of-Sight (NLOS) links generally rely upon reflection of the light from the ceiling or some other diffusely reflecting surface. LOS link design maximizes power efficiency and minimizes multipath distortion. Non-LOS link design increases link robustness and ease of use, allowing the link to operate even when barriers, such as people

or cubicle partitions, stand between the transmitter and receiver. The greatest robustness and ease of use are achieved by the non-directed-non-LOS link design, which is often referred to as a diffuse link.

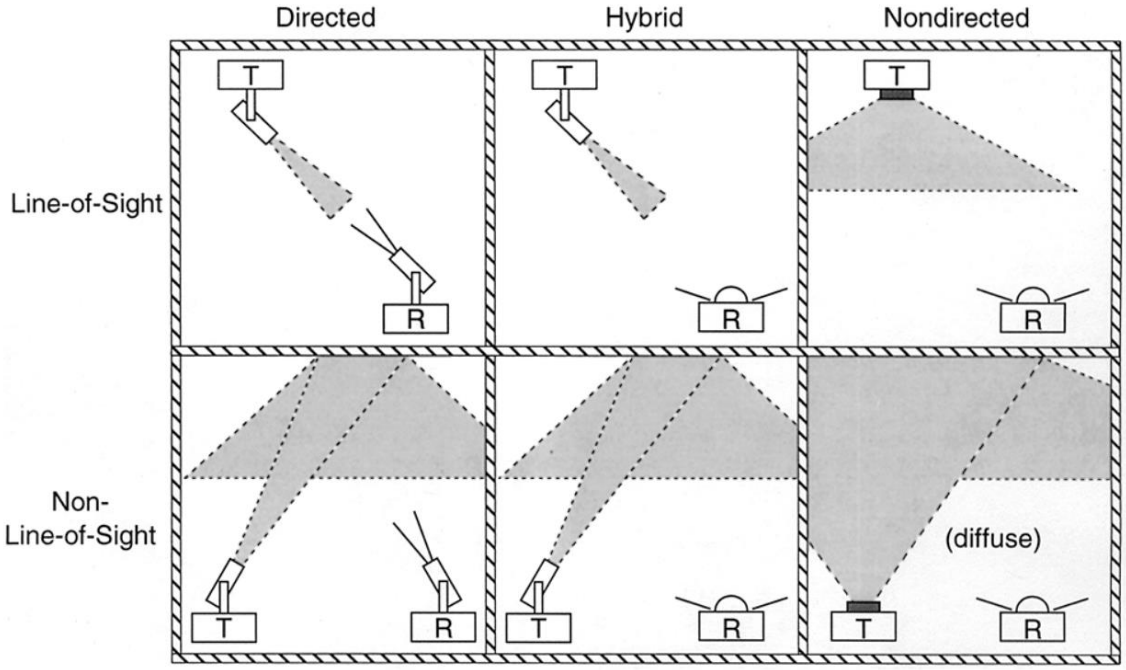

Fig. 1.4 Classification of simple OWC links according to the degree of directionality of the transmitter and receiver and whether the link relies upon the existence of a LOS path between them [15]

This work is focused on the TCP behavior analysis in an indoor environment, considering LOS links. The reason to not consider the NLOS is that the analyzed scenario is indoor scenario and there are no reflecting objects:

This means that the multipath components are almost negligible, except near to the walls, since the light intensity strongly depends on distance.

Intensity Modulation with Direct Detection (IM/DD) is the transmission technique used in optical wireless systems, VLC included [14], [15]. This incoherent method is chosen because of its simplicity and lower cost of implementation compared to coherence schemes used in guided fiber optics.

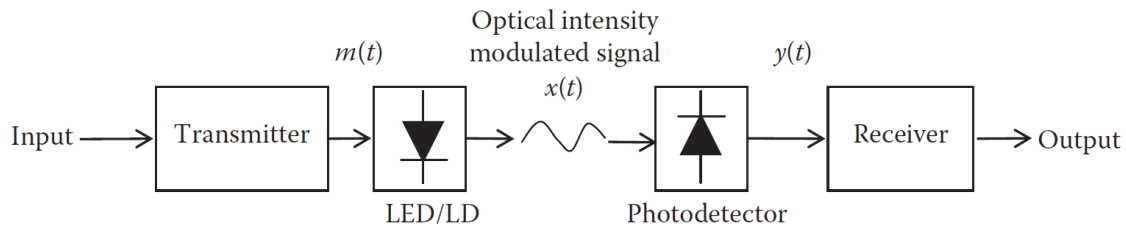

Fig. 1.5 Block diagram of an IM/DD communication channel [16]

In Fig. 1.5 we can see the blocks that compose a IM/DD communication channel [16]: the drive current of the optical source is directly modulated by the modulating signal $m(t)$, which in turn varies the intensity of the optical source $x(t)$. The receiver employs a photodetector with a response, which is the integration of tens of thousands of very short wave-lengths of the incident optical signal, that generates a photocurrent $y(t)$. This photocurrent is directly proportional to the instantaneous optical power incident on it, that is, proportional to the square of the received electric field.

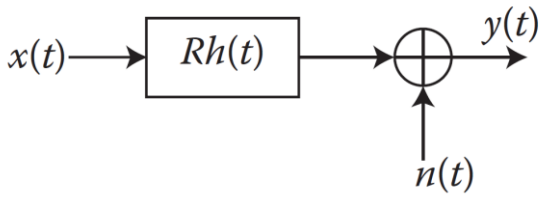

Fig. 1.6 Equivalent baseband model of an optical wireless system using IM/DD [16]

The channel can be modelled as a baseband linear system (see Fig. 1.7):

$$y(t) = Rx(t) \otimes h(t) + n(t) \quad \textbf{(1.1)}$$

Where $y(t)$ is the output current, $x(t)$ the instantaneous input power, R is the is the photodetector responsivity, $h(t)$ the baseband impulse response and $n(t)$ is the noise. In VLC, the noise is the result of several types of interference:

The main ones are the shot noise, produced by the ambient light, and the thermal noise, arisen in the transimpedance amplifier (TIA), that dominates the additive noise at the receiver.

One substantial difference of optical wireless systems over the RF ones is the absence of multipath fading:

As seen in Fig. 1.7, the received electric field generally displays spatial variation of magnitude and phase (due to the multipath propagation in NLOS links), so that “multipath fading” would be experienced if the detector were smaller than a wavelength but, since typical detector areas are millions of square wavelengths, we have spatial diversity that prevents multipath fading. [1]

The total photocurrent generated is proportional to the integral of the optical power over the entire photodetector surface, as showed in Fig. 1.7.

[1] The detector is equivalent to a two-dimensional array of many antennas whose receptions are squared, low-pass filtered, and summed [15]

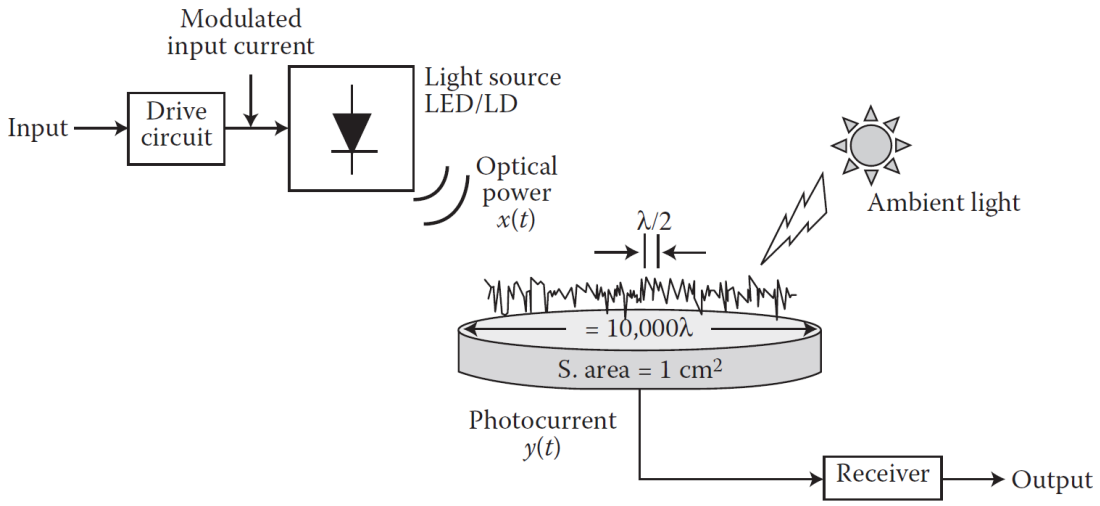

Fig. 1.7 Transmission and reception in an VLC link with IM/DD [16]

Even if indoor VLC links are not affected by the effects of multipath fading, they do suffer from the effects of dispersion, which manifests itself in a practical sense as the Intersymbol Interference (ISI). The dispersion is modelled as a linear baseband channel impulse response $h(t)$. The channel characteristic of an VLC link is fixed for a given position of transmitter, receiver and intervening reflecting objects: it only changes when these components are moved by distances of the order of centimeters [15]. Due to high bit rates, and the relatively slow movement of objects and people within a room, the channel will vary only on the time scale of many bit periods, and may therefore be considered as quasi-static [17].

OWC differs from conventional electrical and radio systems since the instantaneous optical power is proportional to the generated electrical current. $x(t)$ represents power rather than the amplitude signal. This imposes two constraints on the transmitted signal:

- $x(t)$ must be nonnegative ($x(t) \geq 0$)
- A limited maximum transmitted power (to respect the eye safety)

Therefore, because of the eye safety requirement, the average power must be limited to a specified value P_{MAX} and, consequently, also $x(t)$ must be limited too. This contrasts with the time-averaged value of the signal $|\mathrm{x(t)}|^2$, which is the case for the conventional RF channel when $x(t)$ represents amplitude.

1.3.1 Signal-to-Noise Ratio model in VLC

The differences described above have a deep effect on the system design. While in the Signal-to-Noise Ratio (SNR), that in RF channels is proportional to the average received power, in the optical wireless it is proportional to the square of the received optical power signal:

$$SNR = \frac{(P_r R)^2}{\sigma_{total}^2} \quad \textbf{(1.2)}$$

where P_r denotes the average optical power received of the signal, R is the responsivity of the photodetector and $\boldsymbol{\sigma_{total}^2}$ is the total noise variance.

Since the ambient light noise, caused by solar radiation and other illumination sources, is filtered using an electrical high pass filters, the total noise variance is the resultant of the summation of the variance of the shot noise and the variance of the thermal noise:

$$\boldsymbol{\sigma_{total}^2 = \sigma_{shot}^2 + \sigma_{thermal}^2} \quad \textbf{(1.3)}$$

Based on [14], [16] the two terms above can be calculated as :

$$\sigma_{shot}^2 = 2qPRB + 2qI_bI_2B \quad \textbf{(1.4)}$$

$$\boldsymbol{\sigma_{thermal}^2 = \frac{8\pi\kappa T_k}{G_{ol}} C_{pd} A I_2 B^2 + \frac{16\pi^2\kappa T_k \eta}{g_m} C_{pd}^2 A^2 I_3 B^3} \quad \textbf{(1.5)}$$

where B is the bandwidth of the photodetector, κ is the Boltzmann's constant, I_b is the photocurrent due to background radiation, G_{ol} is the open-loop voltage gain, T_k is the absolute temperature, C_{pd} is capacitance of the photodetector per unit area, η is the FET channel noise factor, g_m is the FET transconductance, and I_2 and I_3 are the noise-bandwidth factors with values 0.562 and 0.0868 respectively.

Shot noise and thermal noise are dependent on the area of the photodetector, and depending on factors such as room temperature, ambient light etc. either of them can dominate the overall noise [14] observed by the VLC receiver.

1.3.2 DC gain

Since transmitted signals in VLC are real and positive, relationship between transmitted power and received power can be directly calculated with DC gain $H(0)$ [15]. In addition, in LOS the DC gain can be computed fairly accurately by considering only the LOS propagation path. We consider the link geometry shown in Fig. 1.1.

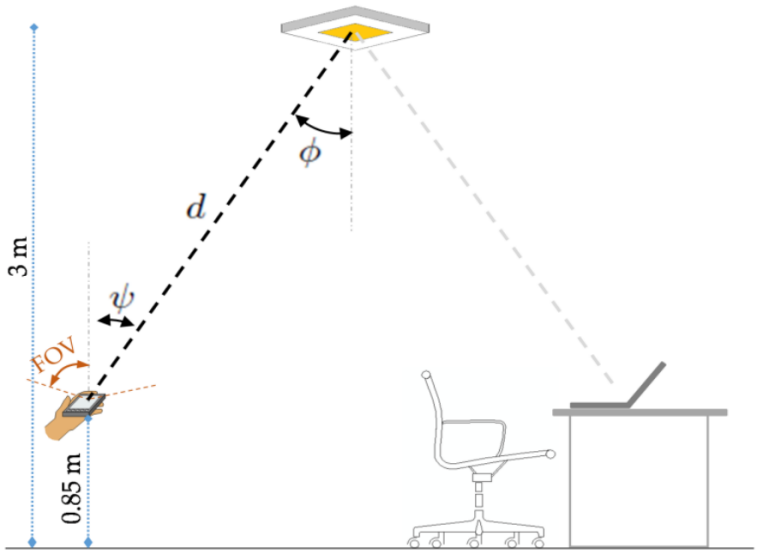

Fig. 1.8 VLC system model and its geometries

Therefore, the received power can be found as

$$\boldsymbol{P_{rx} = H(0)P_{tx}} \tag{1.6}$$

where $\boldsymbol{P_{rx}}$ is the received power and $\boldsymbol{P_{tx}}$ is the transmitted power.
Several LOS components can be sensed by an optical receiver. Therefore, in order to calculate the sum of these components, we utilize generalized Lambertian intensity [18].

The DC channel gain is calculated as follows [15][19]:

$$\boldsymbol{H(0)} = \begin{cases} \frac{(m+1)A}{2\pi d^2}\, cos^m(\phi)\, T_s\, g(\psi) \cos(\psi), & 0 \le \psi \le \psi_c \\ 0, & \psi > \psi_c \end{cases} \tag{1.7}$$

where d is the distance between LED and PD, ϕ is the angle of irradiance at PD, ψ is the angle of incidence at transmitter LED, ψ_c is the width of receiver Field-of-View (FOV), T_s is the gain of the optical filter, A is the area of the detector.
m is the Lambert's mode number expressing directivity of the source beam, $\phi = 0$ is the angle of maximum radiated power. The order of Lambertian emission m is related to the transmitter semi-angle at half-power $\Phi_{1/2}$:

$$\boldsymbol{m = -ln(2)/ln(cos(\Phi_{1/2}))} \tag{1.8}$$

Finally, $g(\psi)$ is the optical concentrator gain given as:

$$g(\psi) = \begin{cases} \frac{n^2}{sin^2(\psi_c)}, & 0 \le \psi \le \psi_c \\ 0, & \psi > \psi_c \end{cases} \quad \textbf{(1.9)}$$

where n is the refractive index of the air.

1.4 Modulation schemes

As we have previously stated in Section 0, one of the main differences between VLC and RF is that, in VLC, data cannot be encoded in phase or amplitude of the light signal because they use incoherent solid-state lighting LEDs as front-end devices (due to their low cost) [20]. This means that the information must be encoded in the varying intensity of the emitting light wave and the demodulation depends on direct detection at the receiver.

Another difference from the other types of communication is that any modulation scheme for VLC should not only achieve higher data rate but should also meet the requirements of perceived light to humans. These requirements about perceived light can be characterized by following two properties:

- **Dimming**: The nowadays LED can be dimmed to an arbitrary level and a user may choose an arbitrary level of dimming depending on the application (different levels of luminance are required depending on the activity performed in the place illuminated [14] [21]) or desired energy savings, but the communication should not be affected by the dimming. Furthermore, considering the fact that the relation between the measured light and the perceived light is non-linear [22] (a lamp that is dimmed 1% of its measured light is perceived to be 10% dimmed by the human eye, as shown in Fig. 1.9), the data should be modulated in such a way that any desired level of dimming is supported

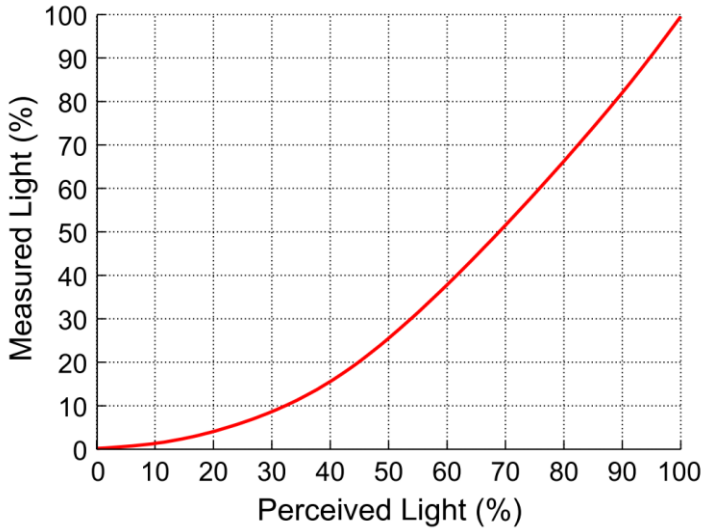

Fig. 1.9 Measured light vs human's eye perceived light

- **Flicker mitigation:** the flickering, that is the changing of the light intensity, can cause serious detrimental physiological changes in humans [23]. Therefore, to avoid that the fluctuations in the brightness of light are perceivable by humans, it's necessary that changes in the light intensity should happen at a rate faster than human eye can perceive. IEEE 802.15.7 standard [24] suggests that flickering (or change in light intensity) should faster than 200 Hz to avoid any harmful effects. This means that any modulation scheme for VLC should mitigate flickering while providing higher data rate.

In Fig. 1.10 it's shown a diagram with the principal modulation techniques for VLC, divided among Single Carrier Modulation Modulations (SCM), Multi-Carrier Modulations (MCM) and Color Domain Modulations.

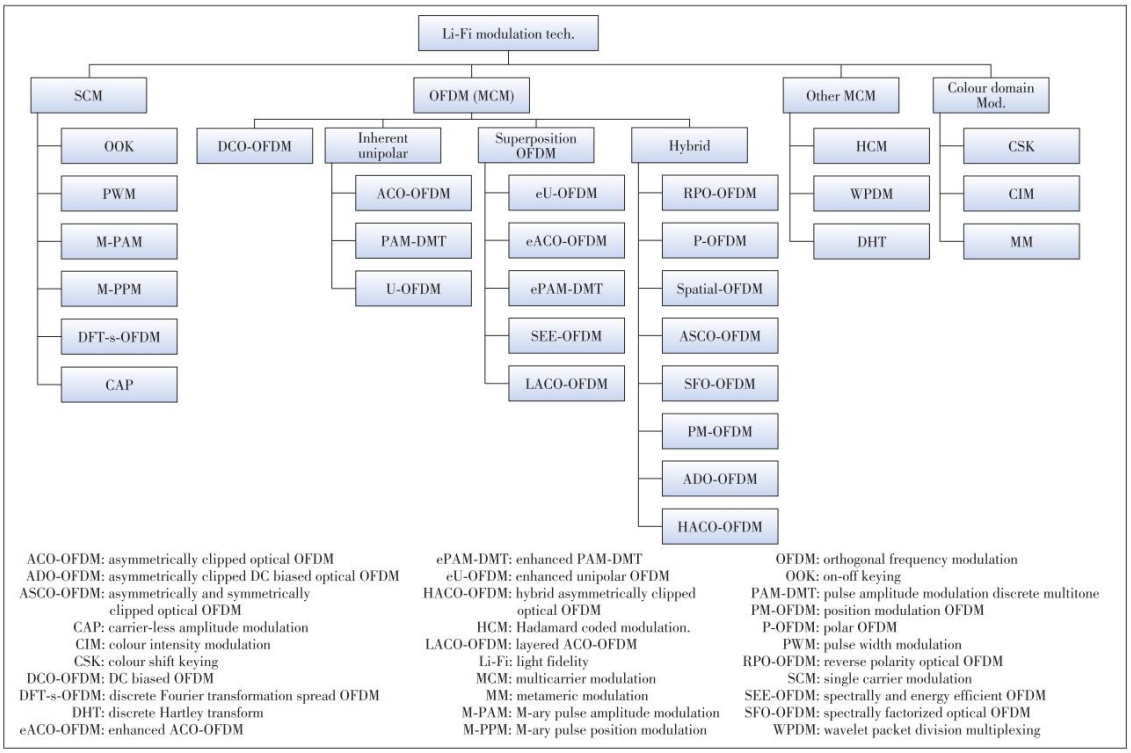

Fig. 1.10 Diagram with some of the VLC modulation techniques [25]

In the following subsections, a summary of the modulation techniques for VLC systems used in this work is presented.

1.4.1 On-Off Keying (OOK)

OOK is one of the simplest and earliest modulation techniques used in OWC and in VLC: the data bits 1 and 0 are transmitted by turning the LED on and off

respectively (in the OFF state, the LED is not completely turned off but rather the light intensity is reduced). Considering a rectangular pulse shape whose duration equals the bit period, the bit error rate (BER) is given by [14]:

$$\boldsymbol{BER_{OOK} = Q\sqrt{SNR}} \quad \textbf{(1.10)}$$

Where $Q(x)$, for a gaussian noise, is:

$$\boldsymbol{Q(x) = \frac{1}{2} erfc\left(\frac{x}{\sqrt{2}}\right)} \quad \textbf{(1.11)}$$

Being $erfc$ the complementary error function.

1.4.2 Pulse Amplitude Modulation methods

PAM is a very basic modulation scheme which is bandwidth efficient. Data is modulated into the amplitude of the signal pulse. This type of modulation is similar to OOK: the main difference with OOK is that the carrier signal has two levels, whereas with PAM, the carrier signal will have 4 or more levels, depending on the modulation order. M-PAM is another notation to indicate it, and M represents the modulation order. In Fig 1.11, a comparison between OOK and M-PAM modulations is illustrated

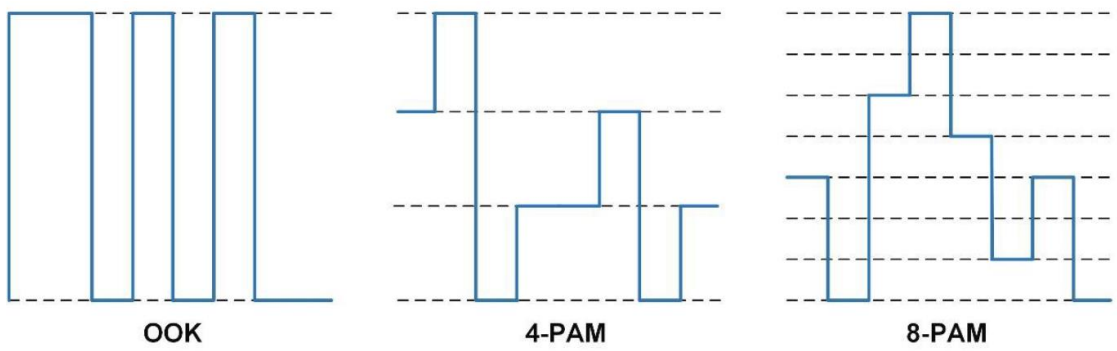

Fig. 1.11 OOK and M-PAM modulation illustration

The Symbol Error Rate (SER) for M-PAM is defined as [26] :

$$\boldsymbol{SER_{M-PAM} = \frac{2(M-1)}{M} Q\left(\frac{\sqrt{SNR}}{M-1}\right)} \quad \textbf{(1.12)}$$

which is similar to Fig. 1.10 considering the term that represents the modulation order. If the modulation order is 2 as in OOK, the expression will be the same as in 1.10. It is important to point out that when we talk about OOK as well as VPPM

(described in next subsection), the bit error rate is the same as the symbol error rate, since each symbol contains only one bit. In the case of M-PAM each symbol has M bits. Therefore, the symbol error rate would be the error associated with the symbols.

Modulation schemes employing multiple intensity levels such as PAM may undergo nonlinearity in LEDs luminous efficacy. Due to the dependence of the color of LED emission on input current and temperature, multiple symbol levels of PAM are subject to shifts in color temperature due to variation in drive current.

1.4.3 Variable Pulse Position Modulation (VPPM)

Variable PPM (VPPM) is a pulse modulation scheme proposed by IEEE 802.15.7 [24] which is a hybrid of Pulse Position Modulation (PPM) and Pulse Width Modulation (PWM).

In PPM, the symbol duration is divided into t slots of equal duration, and a pulse is transmitted into one of the t slots. The position of the pulse identifies the transmitted symbol.

In PWM, the widths of the pulses are adjusted based on the desired level of dimming while pulses themselves carry the modulated signal in the form of a square wave. The modulated signal is transmitted during the pulse, and the LED operates at the full brightness during the pulse. The data rate of the modulated signal should be adjusted based on the dimming requirement. Authors in [45] showed that any dimming level from 0% to 100% can be obtained with high PWM frequency

In VPPM, the bits are encoded by choosing different positions of pulse as in PPM. However, the width of the pulse can also be modified as needed as shown in Fig. 1.12.

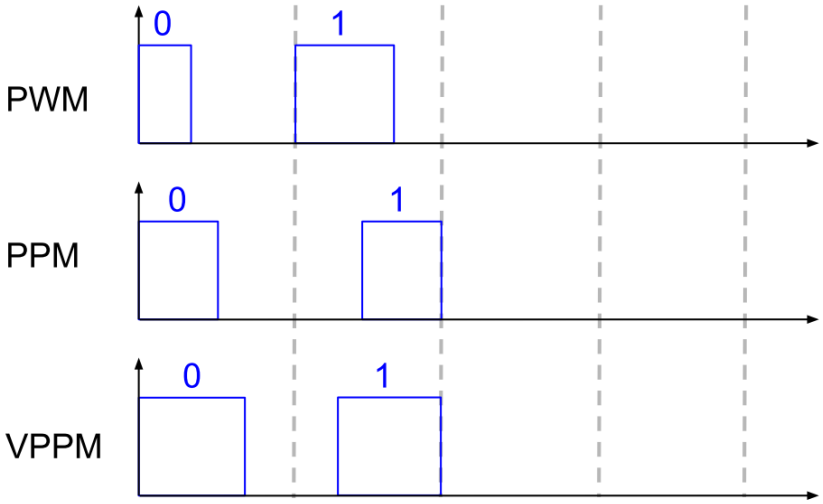

Fig. 1.12 Schematic diagram showing difference between Pulse Width Modulation (PWM), Pulse Position Modulation (PPM) and Variable Pulse Position Modulation (VPPM) [4]

As stated in [24],VPPM makes use of the characteristics of 2-PPM for non-flicker and PWM for dimming control and full brightness. Bits “1” and “0” in VPPM are distinguished by the pulse position within a unit period and have the same pulse width within their respective unit periods. The non-flicker characteristic in VPPM is obtained from the property that the average brightness on bits “1” and “0” is constant. Dimming and full brightness in VPPM are achieved by controlling the “ON” time pulse width. Figure 1.13 describes the dimming control mechanism exploited by VPPM.

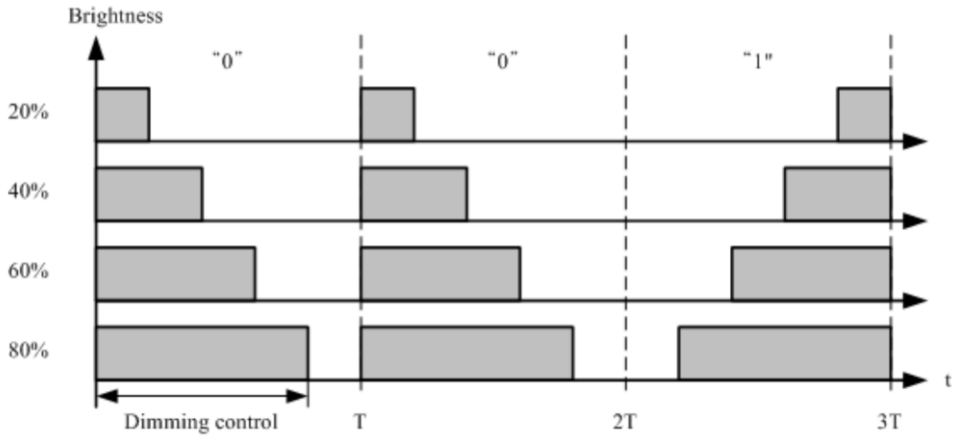

Fig. 1.13 Schematic mechanism for VPPM dimming [24]

According to [26], the BER for the VPPM scheme is :

$$BER_{VPPM} = \begin{cases} Q\sqrt{\frac{SNR}{2b\alpha}}, & \alpha \leq 0.5 \\ Q\sqrt{\frac{SNR(1-\alpha)}{2b\alpha^2}}, & \alpha > 0.5 \end{cases} \quad \textbf{(1.13)}$$

Where α represents the duty cycle of the VPPM signal and b is a factor relating noise bandwidth to symbol rate.

1.4.4 Orthogonal Frequency Division Multiplexing (OFDM)

Techniques such OOK, PPM, PWM and M-PAM can be applied in a relatively straightforward manner. However, as the modulation speeds increases, these modulation schemes begin to suffer from the undesired effects of Intersymbol interference (ISI) due to non-linear frequency response of visible light communication channels. Hence, a more resilient technique is required. OFDM allows adaptive bit and energy loading of different frequency sub-bands according to the communication channel properties [27].

OFDM has been widely adopted in the RF communication due to its ability to effectively combat the inter-symbol interference and multipath fading and it was first proposed for visible light communication in [28]. In OFDM, the channel is divided into multiple orthogonal sub-carrier frequencies, a set of equidistant discrete carriers, which are selected by an Inverse Fast Fourier Transform (IFFT), After that, it succeeds a serial modulation scheme such as M-ary Quadrature Amplitude Modulation (M-QAM) or Phase Shift Keying (M-PSK). IFFT converts the frequency domain input signals into time domain output signals. A cyclic prefix (CP) is added to further limit the effect of ISI.

OFDM for VLC can reduce the inter-symbol interference and it doesn't require complex equalizer. Anyway, there are multiple challenges in realizing its implementation.

First of all, the OFDM technique for RF must to be adapted for application in IM/DD systems such as VLC. This is because OFDM generates complex-valued bipolar signals which need to be converted to real-valued signals. This can be achieved by enforcing Hermitian symmetry constraint on the sub-carriers and then converting the time-domain signals to unipolar signals. Depending on how the bipolar signals are converted to unipolar, there are two types of OFDM techniques:

In Asymmetrically Clipped Optical OFDM (ACO-OFDM), only odd subcarriers are modulated [29] which automatically leads to symmetric time domain signal. While, in DC-biased Optical OFDM (DCO-OFDM) [28], [30] all subcarriers are modulated but a positive direct current is added to make the signal unipolar. In [31] is presented a comparison of both the OFDM schemes and showed that LED clipping distortion is more significant in DCO-OFDM compared to ACO-OFDM.

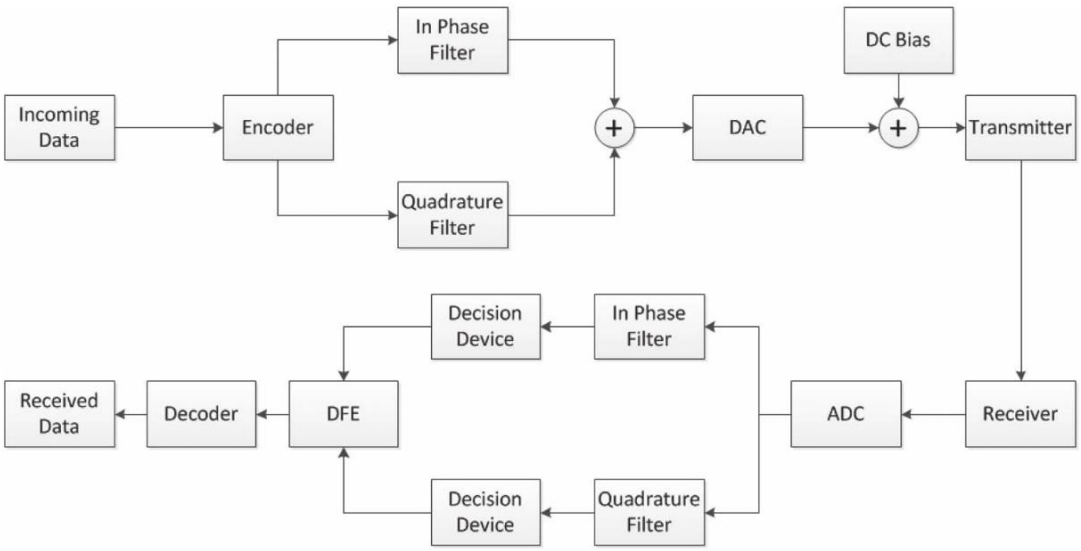

Fig. 1.14 DCO-OFDM system block diagram

The biggest challenge in OFDM VLC system is the nonlinearity of LED [32] since the relationship between the current and the emitted light of the LED is non-linear. This especially affects the OFDM-based VLC systems which have higher Peak-to-Average Power Ratio (PAPR). The effect of this non-linearity was studied in [33], [34] and a solution was proposed to contrast it by operating the LED in a small range where the driving current and optical power are quasi-linear. Apart from the non-linearity, there is only a limited support for dimming [35] in OFDM-based modulation schemes.

Despite these challenges, OFDM for VLC holds great potential with achievable link rates in the scale of multiple Gbps [36] using only a single LED.

In the case of QAM, both the amplitude and the phase of the signal vary. The data stream is formed by M symbols, each composed of k bits from the input. Thus, the constellation is built by $M = 2^k$ symbols which are equal spaced one from another. According to [37], when using an OFDM system with N subcarriers along with M-QAM to modulate each of these subcarriers, being defined as an M-ary QAM OFDM system (M-QAM-N), the BER can be approximated as:

$$\boldsymbol{BER_{M-QAM-N} = \frac{\sqrt{M}-1}{\sqrt{M}\,log_2\sqrt{M}}\,erfc\left(\sqrt{\frac{2^{\sqrt{N}}-1}{2^{\sqrt{N}-1}} \times \frac{3\,log_2 M}{2(M-1)}\,SNR}\right)} \quad \textbf{(1.14)}$$

1.5 Challenges and Opportunities

Based on the review made in [4], some of the important challenges that VLC technology must still address are listed below:

- **FOV Alignment and Shadowing:** For achieving high data rates in VLC links primarily, it is assumed a LOS channel where the transmitter and the receiver have aligned their field of views to maximize the channel response. However, in more practical scenarios, receiver movement and orientation changes are common and the drop in received optical power can be significant due to such misalignment. This requires the design and development of methods that can provide graceful degradation in data rate using the optical power of reflected light.
- **Receiver Design and Energy Efficiency:** Both photodiodes and imaging sensors are currently as VLC signal receivers. The photodiode has a low energy consumption and a small FOV, so it is more suitable for stationary clients, because the FOV can be aligned to the LED fixture. Instead, the imaging sensor have a larger FOV, so they are more robust against movements, but they are slow (due to the higher number of photodiodes) and energy expensive. Thus, it is challenging to design a receiver that can provide robustness to device movements and low-energy use.
- **LED to Internet Connectivity:** In order to create a VLC-based broadband access network, it is necessary to connect the LEDs to Internet. Because the deployment of LEDs (for illumination purposes) is likely to be very dense, it becomes a challenging problem to connect the large number of LEDs to Internet. Deploying wired infrastructure (e.g. Ethernet, fiber, etc.), or using wireless connectivity could nullify the benefits of cost and spectrum highlighted before. Power-line communication could be a solution, as proposed in [38] because it can reuse the existing power line network for communication without additional cost of cable deployment. However, it incurs in cost overheads of using Ethernet-to-power modem and power to VLC modems and there are performance and coverage issues.
- **Uplink and RF Augmentation:** most of the current research work focuses only on the downlink (from LED luminaire to PD/imaging sensor). Although efficient LEDs are incorporated in today's mobile, they cannot be used directly for communication because they would consume a lot of energy and they would cause visual disturbance to users while using the devices. To address this issue, in several works has been proposed the use of other types of communication like RF [39], [40]. Utilizing different communication technologies for uplink and downlink gives rise to heterogeneous networks (HetNets). Such networks impose additional practical challenges such as complex network management for multi-homed clients, throughput asymmetry issues for transport layer, link layer packet loss management and reliable data delivery etc. To build robust high speed HetNet of VLC and RF, it is crucial that these challenges are resolved.
- **Mobility and Coverage:** In order for VLC to be a ubiquitous mobile technology, it must provide uninterrupted and high-speed connectivity in presence of user mobility within a VLC cell and between the VLC cells. Different from RF, even in a small VLC cell, the client SNR varies dramatically (many times within the frame transmission duration) when

user moves within the cell [41]. These fast variations must be accounted for when designing various link-layer techniques such as rate adaptation, frame aggregation, etc. In addition, when VLC is used together with RF networks, user mobility requires seamlessly managing horizontal (VLC to VLC) as well as vertical (VLC to RF) handover of user devices.

In few words, most of the research work has focused on physical and MAC layer performance enhancements with stationary devices: to successfully build and operate a VLC access network, it is imperative to address the issues such as device movement, user mobility and energy efficiency in the design.

CHAPTER 2. TRANSPORT LAYER PROTOCOLS

This chapter contains an overview of TCP and of two congestion control mechanisms it implements, New Reno and Westwood.

2.1 Transport Control Protocol

The Transmission Control Protocol (TCP) is the Internet's transport-layer, connection-oriented, reliable transport protocol. TCP was primarily designed for wired networks, where the BER is negligible and the main cause of packet loss is the congestion.

The main characteristics of TCP are the following:

- It ensures the reliable and ordered delivery of data.
- Before one application process can begin to send data to another using TCP, the two processes must first "handshake" with each other (three-way handshake).
- It provides a full-duplex service, meaning that each TCP connection supports a pair of byte streams, one flowing in each direction.
- A unicast TCP connection is always point-to-point, that is, between a single sender and a single receiver

TCP accepts data from a process through the socket and it directs this data to the connection's send buffer, which is one of the buffers that is set aside during the initial three-way handshake. Then, from time to time, it grabs data from the send buffer and it divides it into chunks, adding a TCP header creating a TCP segment, that is the Protocol Data Unit (PDU) of TCP. After that it calls on the network layer to transmit each segment to the destination TCP, where the data will follow the opposite path. (Fig. 2.15).

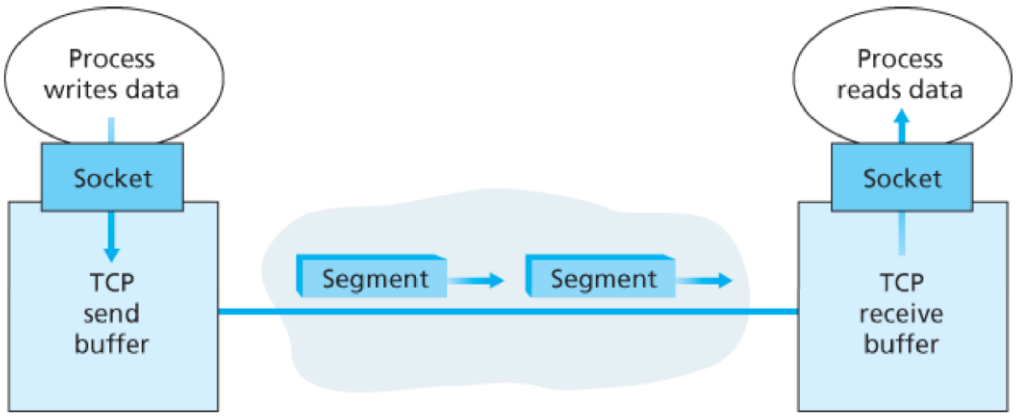

Fig. 2.15 TCP send and receive buffers [42]

A segment is composed by a 20-bytes header (Fig. 2.16) and a variable payload with a maximum size of 65535 bytes. However, this is usually limited by the lower layer protocols. The TCP segment size has a big impact on the packet error rate (PER) of a wireless channel: Reducing this size would decrease the PER, but it would result in a waste of bandwidth or lower utilization of the channel.

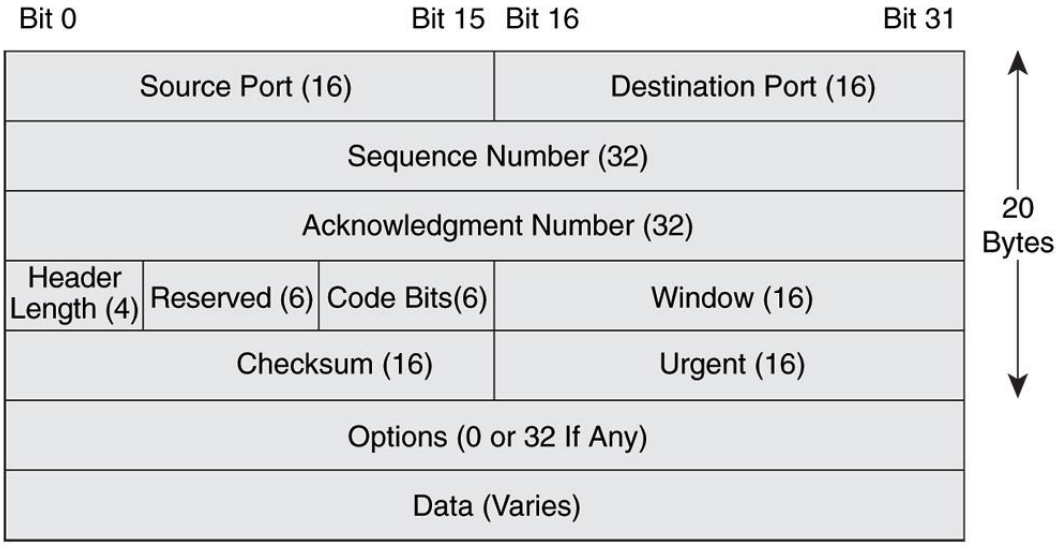

Fig. 2.16 TCP segment structure

2.2 Overview of TCP congestion control mechanisms

As stated before, TCP is a reliable transport layer protocol that uses different mechanisms to avoid and/or to solve the network congestion that, in this case, means the loss of segments and it leads to retransmissions, reduced data throughput and performance degradation. The loss of segments can be due to different causes, depending on the channel type: for example, in wireless channels the packets loss might be caused by interference or poor channel quality.

The TCP congestion-control mechanism operates at the sender and it is based on the congestion window (cwnd), a parameter that imposes a constraint to the amount of data the sender can transmit into the network before receiving an acknowledgement (ACK). Instead, the receiver's advertised window (rwnd) is a receiver-side limit to the amount of outstanding data. The amount of unacknowledged data at a sender may not exceed the minimum of cwnd and rwnd.

There are four main algorithms [43] that support the congestion control strategy of TCP:

- Slow start
- Congestion avoidance
- Fast retransmit
- Fast recovery

With slow start algorithm, when a new connection is established with a host on another network, the congestion window is initialized to one segment. Each time ACKs are received, the congestion window is increased by the number of packets acknowledged, growing exponentially. Instead, in congestion avoidance algorithm, the cwnd is incremented by $segsize * segsize/cwnd$ each time an ACK is received, where segsize is the segment size and cwnd is maintained in bytes (the cwnd has a linear growth).

In both the cases, the process continues until the congestion window reaches a threshold named start threshold size (ssthresh), or congestion occurs (indicated by a timeout or the reception of duplicate ACKs): in the second case, the ssthresh value is set to one-half of the current window size (duplicate ACK's) or it is set to one segment (timeout). When new data is acknowledged by the other end, the cwnd increases depending on whether TCP is performing slow start or congestion avoidance.

The fast-retransmit algorithm allows to recognize when a packet is lost without waiting for the timeout: After receiving a small number (usually 3) of duplicate acknowledgements for the same TCP segment (dup ACKs), the transmitter infers that a packet has been lost and it retransmits the packet without waiting for a retransmission timer to expire, achieving a higher channel utilization and connection throughput. However, the reception of these duplicate ACKs means that there is still flowing between the two ends: so, after the fast-retransmit sends what appears to be the missing segment, the fast recovery algorithm triggers the congestion avoidance, instead of the slow start, allowing a higher throughput under moderate congestion, especially for large windows.

2.3 TCP New Reno

TCP New Reno improves the retransmission process during the fast recovery phase of TCP Reno, the first version of TCP to implement all the four algorithms described above. TCP New Reno can detect multiple packet losses: It does not exit the fast recovery phase until all unacknowledged segments at the time of fast recovery are acknowledged. It implies that in New Reno, partial ACKs do not take TCP out of fast recovery, but they are seen as an indicator that the packet in the sequence space has been lost and should be retransmitted. Therefore, when multiple packets are lost from a single window of data, at this time New Reno can improve without retransmission time out. The retransmitting rate is one packet loss per round trip time until all the lost packets from that window have been

transmitted. It stays in fast recovery till all the data is injected into network, and still waiting for an acknowledgement that fast recovery was initiated.

In this way, it overcomes the problem faced by Reno reducing the congestion window size multiple times in case of multiple packet losses.

The main limitation of New Reno is that it can detect and resend only one packet loss per round-trip-time. This constraint becomes more restrictive as the delay-bandwidth becomes greater.

2.4 TCP Westwood

TCP Westwood is a sender-side-only modification of TCP Reno that uses bandwidth estimation. The congestion window dynamics during slow start and congestion avoidance are unchanged.

The general idea is to use the bandwidth estimate (BWE) to better set the congestion control parameters, congestion window and slow start threshold, after a congestion episode. In TCP Westwood the sender continuously computes the connection BWE as following [44]:

$$\boldsymbol{BWE = \hat{b}_k = \alpha_k \hat{b}_{k-1} + (1 - \alpha_k)\left(\frac{b_k + b_{k-1}}{2}\right)} \quad \textbf{(2.1)}$$

where $\hat{b}_k$ is the filtered continuous first order low-pass filter using the Tustin estimate of the bandwidth at time t_k, $b_k = d_k/(t_k - t_{k-1})$ is the bandwidth sample, $d_k$is the number of bytes acknowledged by ACK k, t_k is the arrival time of ACK k, $\alpha_k = \frac{2\tau - (t_k - t_{k-1})}{2\tau - (t_k - t_{k-1})}$ is the time varying exponential filter coefficient at t_k and $1/\tau$ is the filter cut-off frequency of this Tustin filter.

Thus, BWE is equal to the average rate at which data is delivered to the TCP receiver and it is based on ACK arrival times and the increment of data delivered to the destination. After a packet loss, the congestion window is set to $BWE \times RTT_{min}$, where RTT_{min} is the minimum round-trip delay experienced by the connection.

TCP Westwood is very effective in handling wireless loss [45]. This is because Westwood uses the current estimated rate as reference for resetting the congestion window. The current rate is only marginally impacted by loss (as long as loss is a relatively small fraction of data rate).

CHAPTER 3. SIMULATION ENVIRONMENT

This chapter starts with a small review of the available simulation environments, followed by a brief overview of the NS3 framework. Then, the design and implementation of two different NS3 modules are presented. Finally, the simulation scenarios are introduced.

3.1 Simulation tools

When it comes to study the behavior of a communication system, we can divide its functions in abstract layers following the Open System Interconnection (OSI) model:

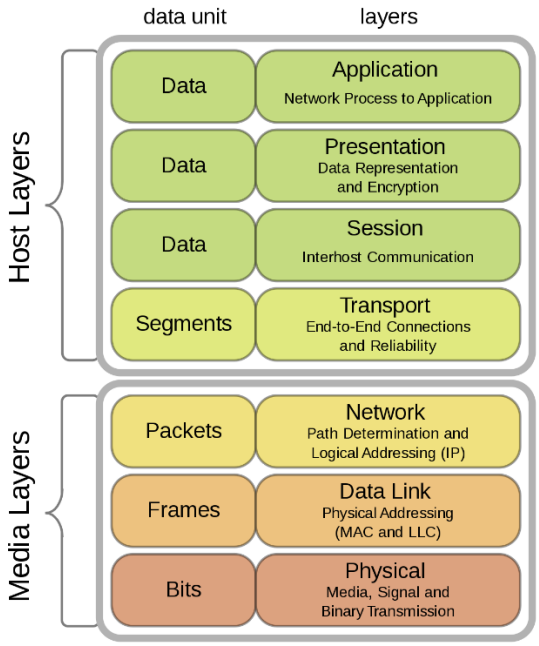

Fig. 3.17 OSI model (source Wikipedia)

The final goal of this work is to analyze the behavior of the TCP, but the attention was also focused on the lower layers, especially on the Physical layer. This is a significant problem when it comes to choose the simulation environment because they usually focus on just one of these layers.

Network simulators, like ns-2, ns-3 and OMNET++, abstract the physical layer and consider the frame/packet as an indivisible unit, thereby ignoring (channel) effects on individual bits as well as specific coding and signal processing details. On the other hand, physical layer simulators (like MATLAB and IT++) do not readily consider network characteristics, nor do they reflect the functionality of medium access or network layer protocols.

This separation of concerns can lead to unconsidered, or inappropriately modelled effects in network layer studies and to imprecise assumptions in physical layer research. A solution to this issue is given in [46] for the case of the Vehicular Communication Networks, but it is valid in general:

They integrated a physical layer simulator, IT++, into a network simulator, ns-3, reaching a higher accuracy at the cost of an increased computational cost (mainly due to the complex channel models).

In this thesis, the choice has been that one of continuing the work started in [47] with ns-3 and to create a more flexible and reliable Physical layer, without the use of an external physical layer simulator.

3.2 NS3 framework

ns-3 is an open-source discrete-event network simulator for research and educational use [48]. Even if its name recalls another famous network simulator, ns-2, it is not its new version, but a completely new tool designed to replace it.

The ns-3 project is committed to building a solid simulation core that is well documented, easy to use and debug, and that supplies to the needs of the entire simulation workflow, from simulation configuration to trace collection and analysis.

As stated in [49], one of the fundamental goals in the ns-3 design was to improve the realism of the models: others decided to use high-level modeling languages and simulation-specific programming paradigms, losing the model accuracy and producing simulation results diverged too much from experimental results. Instead, ns-3 developers chose C++ as programming language, to better facilitate the inclusion of C-based implementation, and an architecture similar to the one used in Linux devices (with internal interfaces -network to device driver- and application interfaces -sockets-) with the goal of reducing the possible discontinuities when moving from simulation to experiment.

3.2.1 Network element models

Here we list the main models that ns-3 use to abstract all the various network elements:

- **Node:** representation of a network device (both end-systems such as mobile terminals, as well as network routers, hubs and switches) where different functionality can be added such as protocol stacks, peripheral cards, or mobility functions.
- **Net-Device:** the physical device that connects a node to the communications channel. It must be installed in a node and acts as a peripheral card or Network Interface Card (NIC).

- **Channel:** it represents the medium used to send the information between network devices (the communication channel). These might be fiber-optic point-to-point links, shared broadcast-based media such as Ethernet, or the wireless spectrum used for wireless communications.
- **Communications protocols:** they model the implementation of protocol descriptions found in the various Internet Request for Comments documents, as well as newer experimental protocols not yet standardized.
- **Protocol headers:** which are subsets of the data found in network packets and have specific formats for each of the protocol objects they are associated with.
- **Network packets:** they are the fundamental unit of information exchange in computer networks, so they are also the fundamental unit of ns-3.

In addition to the models for the network elements mentioned above, ns-3 has several helper objects that assist in the execution and analysis of the simulation but are not directly modelled in the simulation. These are:

- **Random variables generator**: random variables can be created and sampled to add the necessary randomness in the simulation. Various distributions are provided, including uniform, normal, exponential, Pareto, and Weibull.
- **Trace objects:** they facilitate the logging of performance data during the execution of the simulation, that can be used for later performance analysis. Trace objects can be connected to nearly any of the other network element models and can create the trace information in several different formats (e.g. the packet capture log, known as *pcap*).
- **Helper objects:** they are designed to assist with and hide some of the details for various actions needed to create and execute an ns-3 simulation (e.g. the Point to Point Helper provides an easy method to create a point–to–point network).
- **Attributes**: they are used to configure in an easy way most of the network element models with a reasonable set of default values (e.g. the initial time–to–live TTL value specified when a new IPv4 packet is created). It is, of course, possible to change them at runtime.

3.3 VLC module design for NS3

ns-3 software is organized into separate **modules,** each of which is built as a separate software library. Individual ns-3 programs can link the modules (libraries) they need to conduct their simulation. In Fig. 3.18 we can see the core modules of ns-3 that are linked by the others.

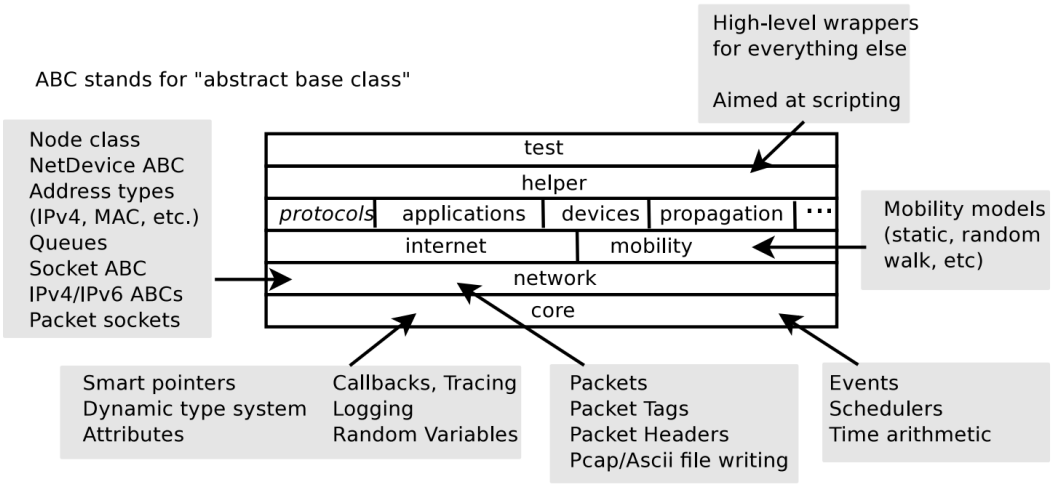

Fig. 3.18 Software organization of ns-3

Modules are different from ns-3 models which are abstract representations of real-world objects, protocols, devices, etc. An ns-3 module may consist of more than one model.

All modules can be found in the *src* directory. Each module can be found in a directory that has the same name as the module. Ns-3 doesn't support natively VLC, even if there have been several researchers who used it to simulate VLC networks. Nevertheless, the only ones who released their code were the authors of [26] who made a new module, characterizing the VLC channel, on the base of Point to Point module.

In this thesis, it has been used an improved implementation of the work in [47] for testing the TCP performances in a network with one access point and one mobile node. Then, a new module has been implemented to support more complex scenarios with several access points and users.

3.3.1 VLC module

In [47], the author created some classes in the Network module in order to implement support the VLC network. These classes are based on the *point-to-point* module, as in [26].

One of the first step was to separate these classes from the *network* module, and to create a new module to make the environment clearer and faster:

The *network* module is part of the ns-3 core and it shouldn't be modified for these purposes. In addition, each small change in one of these classes leads to a longer time when building the project, because of all the classes linked to this module. For these reasons, the *vlc-p2p* was created following the structure indicated for the new modules in ns-3 documentation Fig. 3.19:

```
src/
  module-name/
    bindings/
    doc/
    examples/
      wscript
    helper/
    model/
    test/
      examples-to-run.py
    wscript
```

Fig. 3.19 Module structure

Then, some methods have been added to allow a finer tuning of the channel and devices parameters.

The classes implemented, represented in Fig 3.4, are:

- **VLC_Channel** contains the attributes that define the VLC channel as previously presented in Section1.3. As mentioned before, the channel is derived from the already implemented point-to-point Channel in NS-3. Therefore, only two network devices would be connected to the channel at the same time, in duplex mode.
- **VLC_NetDevice**, based on the point-to-point NetDevice object already existent in NS-3, has the variables and methods to define a VLC network device, such as address and data rate. It also contains the methods that start, end transmission, set tags and manage queues.
- **VLC_SNR** is the class where the signal-to-noise ratio model previously referred and established in Section 1.3 is implemented. In this class it is possible to find the methods required to calculate shot and thermal noise variance, and the signal to noise ratio.
- **VLC_ErrorModel** class basically contains an implementation of the various models proposed in Section 1.4 to calculate BER or SER according to the different modulation techniques addressed in the present research.
- **VLC_TrafficApp** defines a basic application that generates data packets and allows the manipulation of parameters such as the data rate of the source, the length of each packet, and the total number of packets to be generated.

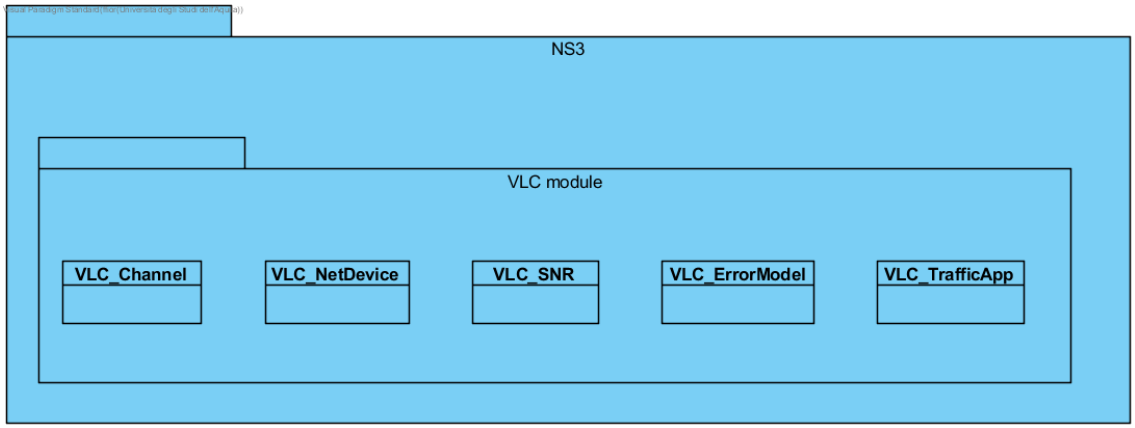

Fig. 3.20 VLC module structure

Finally, one major bug fix has been implemented:

While running simulation tests of a user moving with a random walk mobility model, it was clear that there wasn't any control that the access point was in the receiver's FOV. This leaded to a wrong model of the channel parameters and, consequently, to an erroneous simulation.

To fix this misbehavior, it was implemented a check to apply correctly the formula 1.7, considering the transmitters and receiver position, with their FOV, at each time step.

3.3.2 LiFi module

The VLC module has several restrictions, being the limit of only two devices for channel one of the more important.

Another relevant constraint comes when using multicarrier modulation schemes, like OFDM:

With this type of modulation, when the communication is divided over several subcarriers, each one can experience different channel quality due to, for example, frequency-dependent interference patterns. Hence, using the same modulation and coding schemes for all subcarriers (the module doesn't abstract the concept of subcarrier) would yield sub-optimal performance, since the subcarriers typically experience different SNR values.

For the reasons explained above, and because of the big interest that optical OFDM is collecting due to his high performances [36] and his inclusion in the new IEEE standard [50], it has been decided to implement a new spectrum-aware module for emulating a LiFi system using the framework presented in [51], the same that has been used to implement the LTE and WIFI module.

The Fig. 3.212 shows the model classes of the LiFi module. These are:

- **LifiAntenna:** this class, inherited from the ns3 *Antenna model*, implements a model of VLC "antenna", meaning a device able to transmit

and receive a VLC signal. It models all the parameters described in the Subsection 1.3.2 for the calculation of the DC gain.

- **LifiSpectrumChannel:** it represents the channel with its characteristics. This class is intended to dispatch transmissions between PHY layers, but also to host channel propagation models.
- **LifiSpectrumPhy:** it represents the Physical layer implementation of the NetDevice and the interface to communicate with the channel. Thanks to spectrum model, it allows to calculate the SNR for each subcarrier. This PHY layer implementation, derived by HalfDuplexIdealPhy class, realizes an ideal OFDM PHY which transmits half-duplex. The device is ideal in the sense that:
    - it uses an error model based on the Shannon capacity, which assumes ideal channel coding;
    - it uses ideal signal acquisition, i.e., preamble detection and synchronization are always successful
    - it has no PHY layer overhead
- **LifiSpectrumInterference:** it implements the model interference used by the LifiSpectrumPhy. In this case, a Gaussian interference model is implemented. It is also in charge of calculating the Signal-to-Interference-plus-Noise Ratio (SINR).
- **LifiSpectrumError:** it is the class that calculates the Packet Error Rate, based on the SER formula described in Section 1.4.
- **LifiNetDevice:** it is based on the AlohaNoackNetDevice. It is a minimal NetDevice that allows to send packets over LifiSpectrumPhy and it implements the following features:
    - layer 3 protocol multiplexing
    - MAC addressing
    - Aloha MAC

In Fig. 3.22, the sequence diagram shows all the process for sending a packet, illustrating the interaction among all the classes involved. The parameters passed in the methods are:

- **Packet:** it is the reference to packet that must be transmitted
- **SPD:** it is the Spectral Power Density of the signal transmitted
- **spd_duration:** it is the duration in seconds of the signal transmitted
- **signal_parameters:** it collects all the parameters above

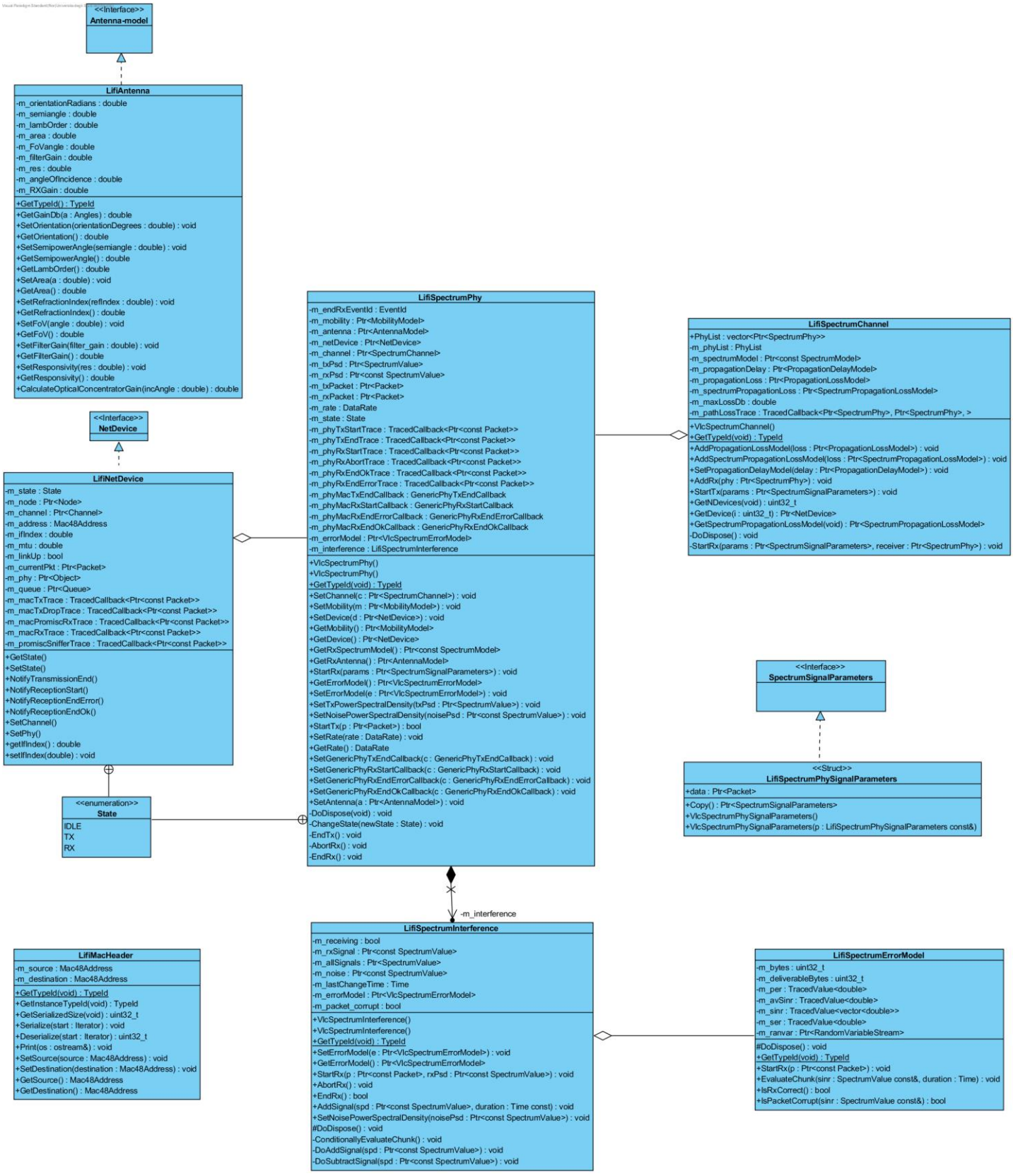

Fig. 3.21 VLC module's class diagram

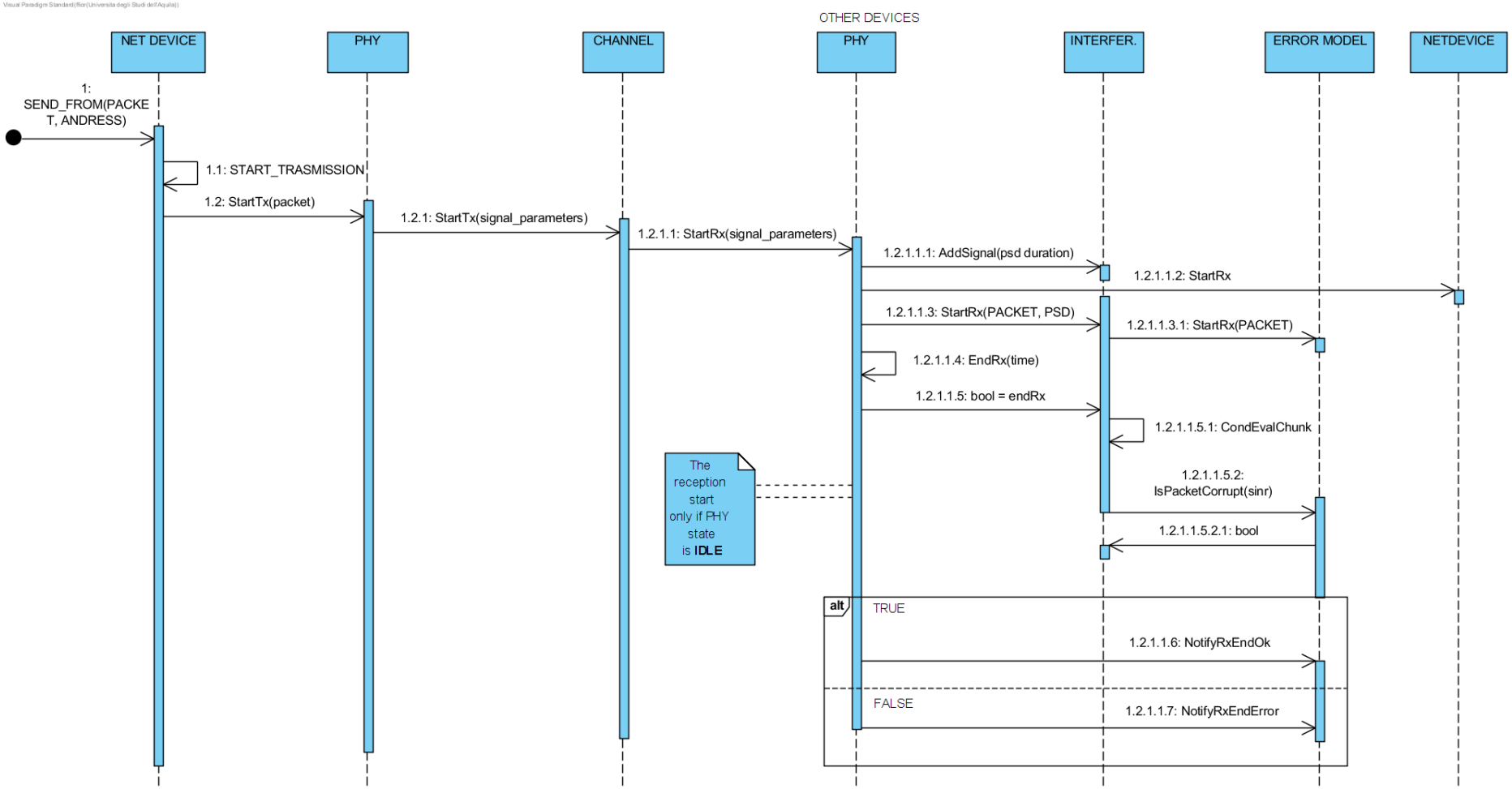

Fig. 3.22 Packet transmission sequence diagram

3.4 Simulation scenarios

There are two different simulation scenarios. The main one is showed in Fig. 3.23 and it is composed as follows:
There is just one LED bulb/Access Point that is placed in the ceiling of the room, at 3 meters of altitude. The user/Mobile Device moves on a horizontal plane that is imaginarily located at 0.85 m above the floor level, trying to exemplify the common height of a desk in an office. The orientation of the device is fixed, with no rotation. There are no walls and no other objects that can reflect the light, so we can consider just LOS signals.

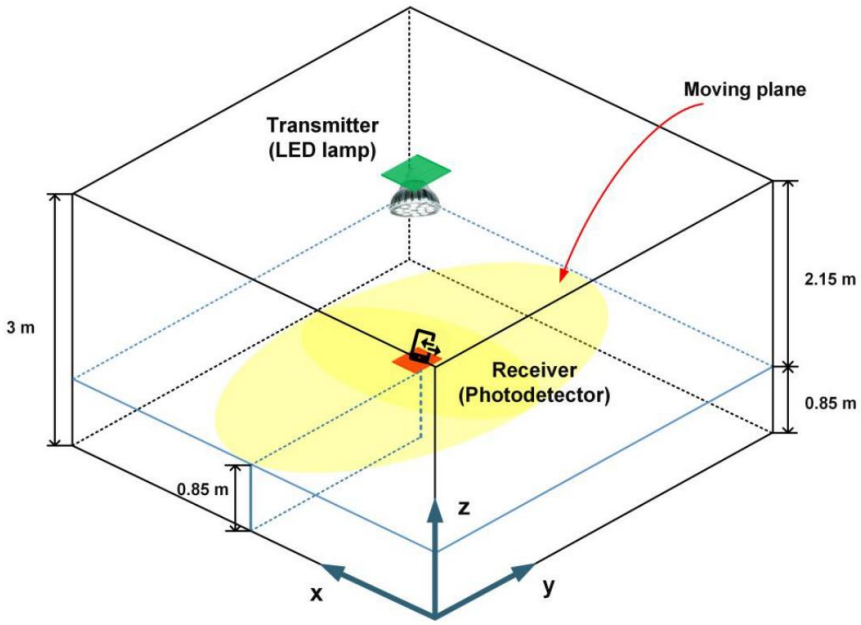

Fig. 3.23 Scheme of the first simulation scenario [47]

The other scenario considers the use of several luminaires, and consequently, Access Points. The 13 LED bulbs are located on the ceiling and they are disposed as illustrated in Fig. 3.24. The height of the ceiling and user plane are the same as in the first scenario, as are valid all the observations made.

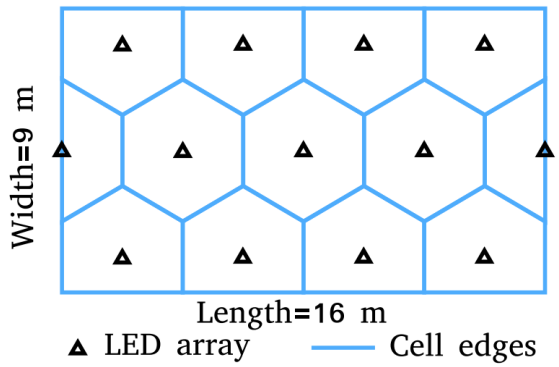

Fig. 3.24 LEDs arrangement in the second scenario

Taking advantage of the mobility models included in ns-3, different subcases can be simulated within this context: the models that will be used are the random walk and the waypoint.

Finally, other tools like Flow Monitor and Wireshark have been used to analyze the results of the simulations.

CHAPTER 4. RESULTS

This chapter presents the results obtained by simulating the scenarios previously described. They are divided in two main sections, one for each developed module. The first one addressed to the VLC module. The parameters related to the VLC channel are shown, such as received power and signal-to-noise ratio; then, the results regarding the behavior of the TCP protocol over this basic VLC network are presented, including a comparison between TCP New Reno and TCP Westwood for various use cases.

The second one is related to the LiFi module which shows the validation of this module, reproducing the results of a well-known paper and making some tests at network and transport layer.

For each scenario, the results are described and analyzed throughout the chapter.

4.1 VLC module results

Since this work continues the one in [47] and, as stated in Section 3.3.1 VLC module, this module is based on the implementation made in that work, the same parameters will be used. It is important to remember that the main purpose of the present work is to analyze the performance of TCP protocol over VLC channel. The channel used is the one described in Section 1.3 Channel model, assuming a LOS between transmitter and receiver. The receiver moves in the x, y plane located at $0.85\ m$ from the ground, bounded to $(-8\ m$ to $+8\ m)$ in both axes, and the receiver plane is always parallel to the transmitter plane.

4.1.1 Received power and SNR

The received power is calculated using the parameters in Table 4.1

Table 4.1 Simulation parameters for received power calculation

	Parameter	Value
Transmitter	Transmitted Power	$72\ W$
	Semi-angle Half Power	$70° - 30°$
	Positions Coordinates (x, y, z)	$(0, 0, 3)\ m$
Receiver	Photodetector Active Area	$1\ \mathrm{cm}^2$
	Field of View Angle	$70° - 30°$
	Refractive Index	1.5
	Optical Filter Gain	1
	Photodetector Responsivity	$0.28\ A/W$
	Positions Coordinates (x, y, z)	$(x, y, 0.85)\ m$

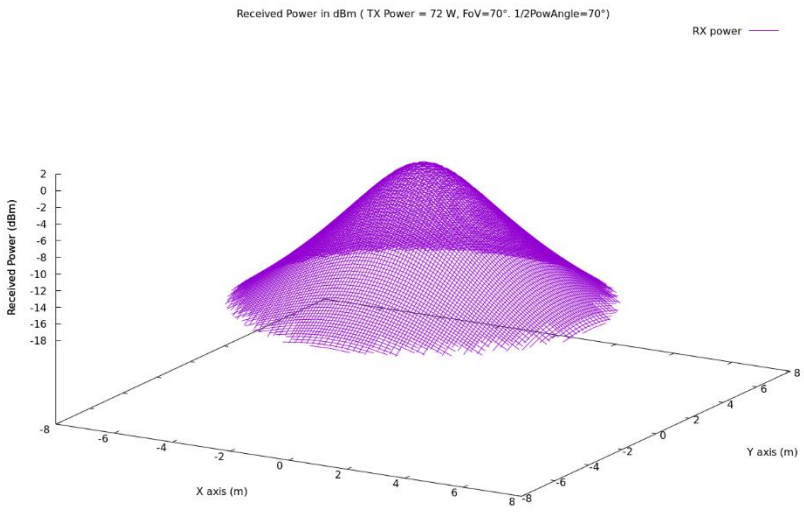

Fig. 4.25 Received power in dBm obtained using transmitted power $P_{tx} = 72W$, Semi-angle Half Power $\Phi_{1/2} = 70°$ and $FOV = 70°$

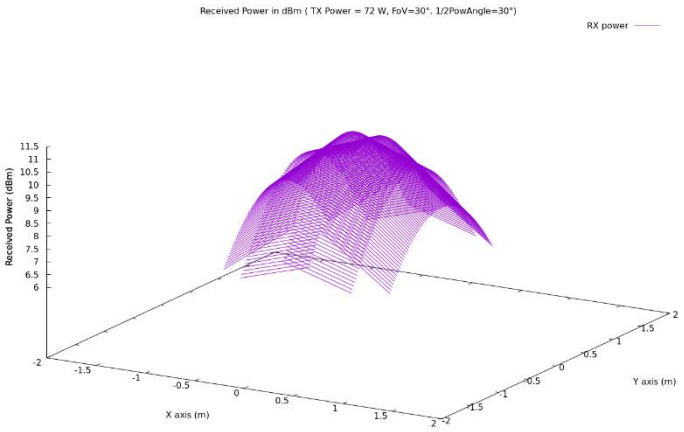

Fig. 4.26 Received power in dBm obtained using transmitted power $P_{tx} = 72W$, Semi-angle Half Power $\Phi_{1/2} = 30°$ and $FOV = 30°$

As expected, the received optical power decreases as the distance to the light source increases. Nevertheless, we can notice that semi-angle at half-power and FOV angle of the receiver are important factors because they basically determine the coverage area of the light source and the range values received power (these angles are defined by the electronic devices and can be found in the data sheets).

The same scenarios have been used to measure the Signal-to-Noise-Ratio, adding the parameters contained in Table 4.2.

Table 4.2 Simulation parameters for SNR calculation

	Parameter	Value
System	Photodiode Responsivity	$0.4\ A/W$
	Absolute Temperature	$24.85\ °C\ (298\ °K)$
	Electronic Noise Bandwidth	$5\ MHz$
	Noise-bandwidth factor I2	0.562
	Fixed Capacitance of Photo Detector	$112\ \frac{pF}{cm^2}$
	Background Current	$5.1\ mA$
	Optical Filter Gain	0.868
	FET Transconductance	$30\ mS$

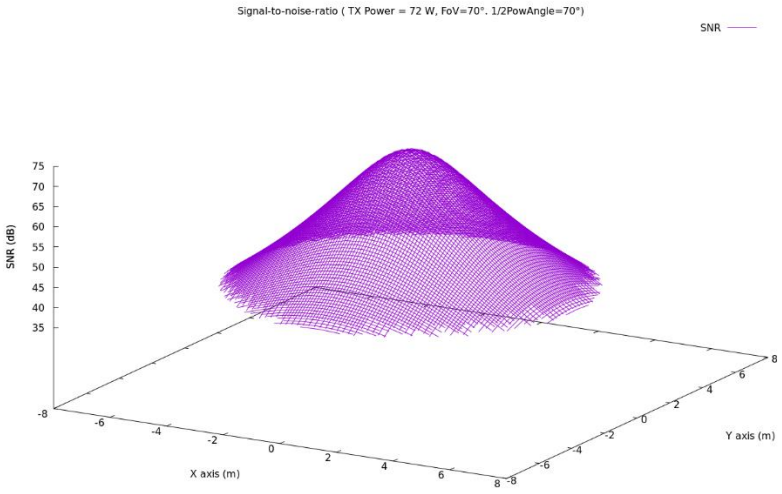

Fig. 4.27 SNR in dB obtained using transmitted power $P_{tx} = 72W$, Semi-angle Half Power $\Phi_{1/2} = 70°$ and $FOV = 70°$

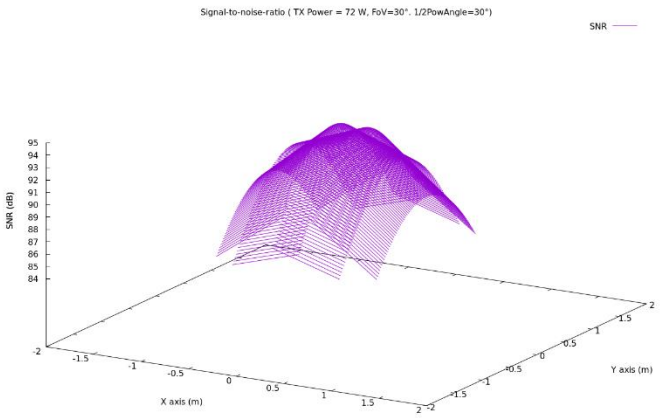

Fig. 4.28 SNR in dB obtained using transmitted power $P_{tx} = 72W$, Semi-angle Half Power $\Phi_{1/2} = 30°$ and $FOV = 30°$

As the relations in Section 1.3.1 Signal-to-Noise Ratio model in VLCanticipated, the patterns are similar to the ones showed in Fig. 4.25 and in Fig. 4.26.

In accordance with the previous results, the smaller are the angles, the greater is the maximum SNR when the receiver is located just below the light source. Nonetheless, the SNR decreases faster as the receiver moves towards the boundaries, compared to the previous scenario.

Finally, it must be underlined that, when the receiver goes out of the field of view, it doesn't receive any longer the signal and both the received power and the SNR become null.

4.1.2 TCP performance

This section is focused on the analysis of the TCP performance over the VLC channel. To continue the work in [47], it has been decided to analyze the scenario where the user moves around the boundaries of the area covered by the access point following a random walk model with a constant speed. Based on the results showed in the same work, where different modulation techniques have been compared, it has been decided to focus on ODFM M-QAM, because it showed the best performances.

The two TCP congestion control algorithms considered are the ones described in chapter 2: New Reno and Westwood. The reason of this choice is that New Reno is one the leading Internet congestion control algorithm, while Westwood is proposed as the best solution for the wireless systems: it is expected that Westwood, that doesn't misinterpret the sporadic losses due to wireless channel problems as a symptom of congestion, will perform better than New Reno.

In Table 4.3 the simulation parameters are shown (the parameters not included in this table, have been already presented in Table 4.1 and Table 4.2).

Table 4.3 Simulation Parameters for TCP performance analysis

	Parameter	Value
Transmitter	Transmitted Power	$72\ W$
	Semi-angle Half Power	$70°$
Receiver	Photodetector Active Area	$1\ \mathrm{cm}^2$
	Field of View Angle	$70°$
System	Bandwidth	$10\ MHz$
	Number of Subcarriers	1
	Modulation Scheme	$16\ QAM$
	Channel data rate	$10\ Mbps$
	Channel delay	$2\ ms$

Source data rate	$8\ Mbps\ (CBR)$
TCP segment size	$1460\ bytes$
Sampling rate	$20\ samples/s$
Simulation execution time	$100\ s$

A constant bit-rate (CBR) application is used to emulate the traffic profile of the emitter. The value of the delay was set to $2\ ms$ considering the propagation over the light channel and also assuming that the data source is not in the same place as the transmitter.

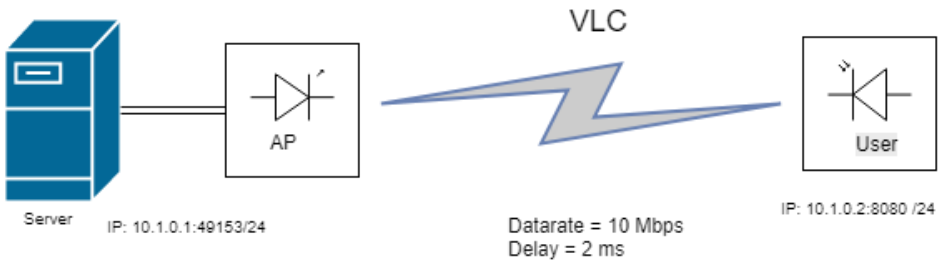

Fig. 4.29 Simulation scenario with one AP and one user

The scheme in Fig. 4.29 represents the network topology of the simulation scenario, including IP addresses and ports, and it shows the path for the end-to-end RTT. This topology has been used to evaluate the performances of the two congestion control algorithms by changing the following parameters:

- TCP sender buffer size
- Channel delay
- Source application data rate

The parameters analyzed are the throughput, the number of dropped packets, the congestion window size and the end-to-end delay.

Before to check the throughput and the other parameters related to TCP performance, Fig. 4.30 shows the SNR value for each position of the receiver during the simulation. Thanks to this picture, it's possible to know when the connection falls because the transmitter is outside the FOV of the receiver.

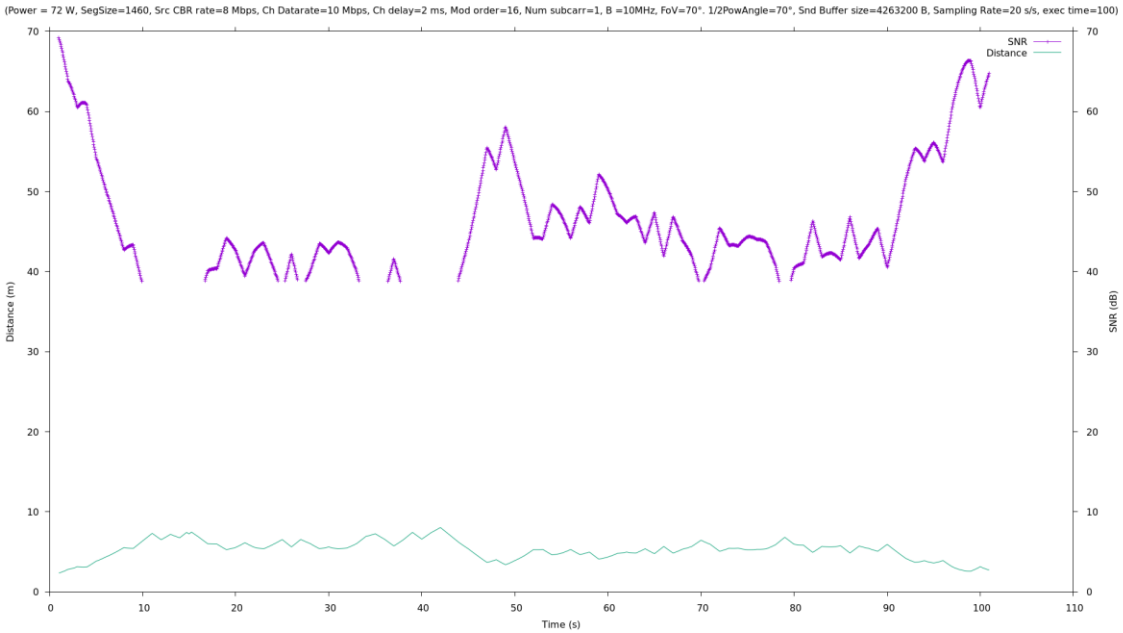

Fig. 4.30 SNR value when the user has random walk mobility model

Sender buffer size

Three different sender buffer sizes for the TCP socket have been used for the tests: 14600, 4263200 and 42632000 Bytes that are, respectively, 10, 2920 and 29200 times the segment size used. Using the Flow Monitor tool, we can analyze the performance using these different buffer sizes and the two congestion control algorithms:

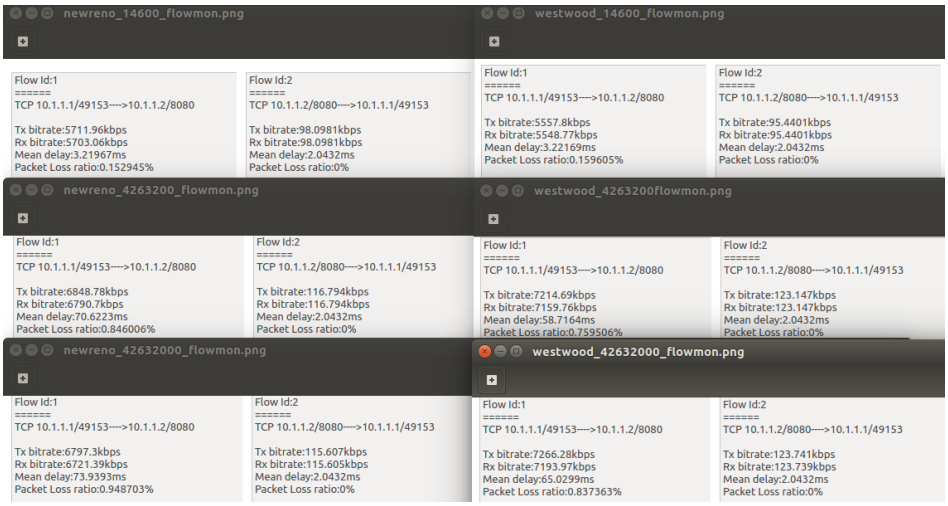

Fig. 4.31 Comparison using different sender buffer sizes and TCP modes

The Fig. 4.31 shows that the average throughput increases with the sender buffer size, as also the mean delay. The higher throughput is due to the fact that the channel data rate is set to 10 Mbps, while the source app data rate is 8 Mbps: when using a big buffer, the instantaneous throughput is higher than the source data rate, as shown in Fig. 4.32, and the average throughput increases.

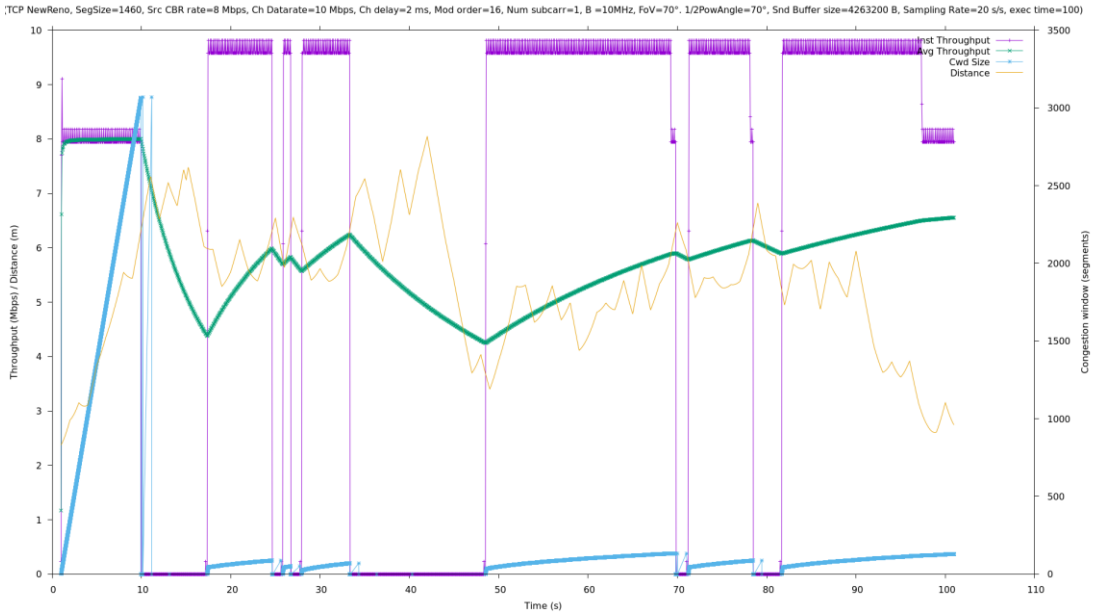

Fig. 4.32 Instantaneous throughput using New Reno and sender buffer size = 4263200 Bytes.

About the increasing in the mean delay, the reason is the following: since the mean delay is calculated as "the sum of all end-to-end delays for all received packets of the flow, divided by the number of received packets", having a higher number of packets stored during the disconnection it will increase significantly the average. It's possible to check this statement in Fig. 4.33.

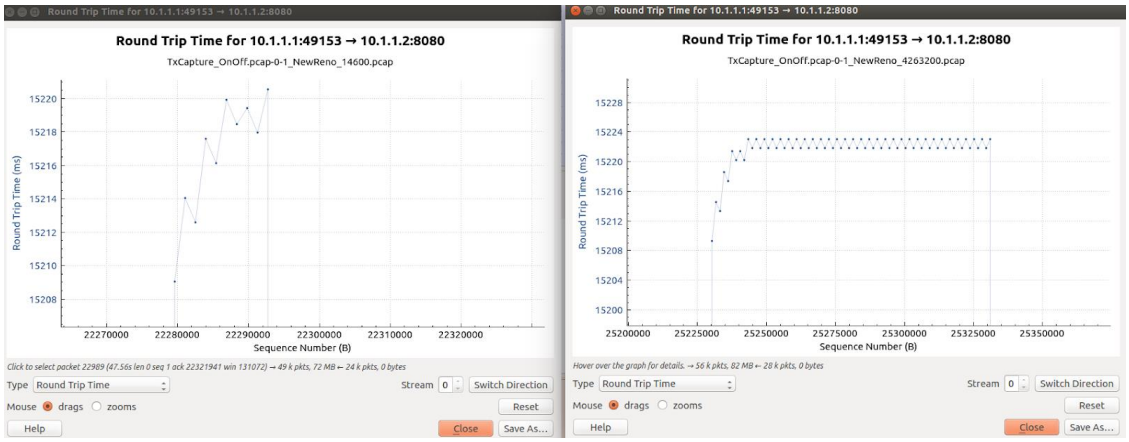

Fig. 4.33 RTT for each packet using New Reno. On the left, sender buffer = 14600 Bytes. On the right, sender buffer = 4263200 Bytes.

About the differences between New Reno and Westwood, it's important to highlight how Westwood performs better in terms of average throughput and mean delay when a big buffer size (e.g. 4263200) is used.

Channel delay

Two different delay values, 2ms and 10ms, and sender buffer sizes, 14600 B and 4263200 B, have been used.

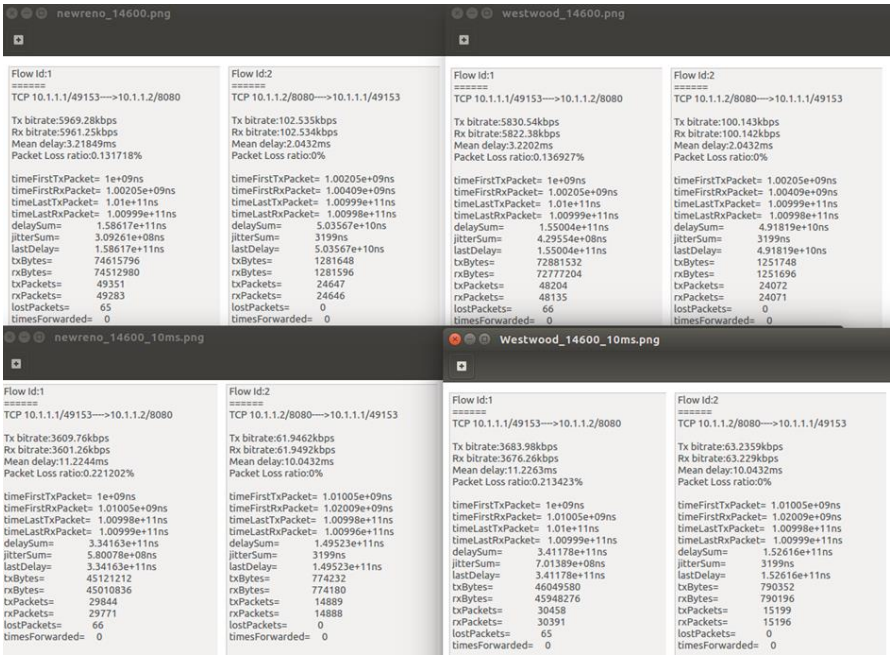

Fig. 4.34 Comparison using a sender buffer size=14600 Bytes and different delay values and TCP modes. On the top the delay is 2ms, on the bottom is 10ms.

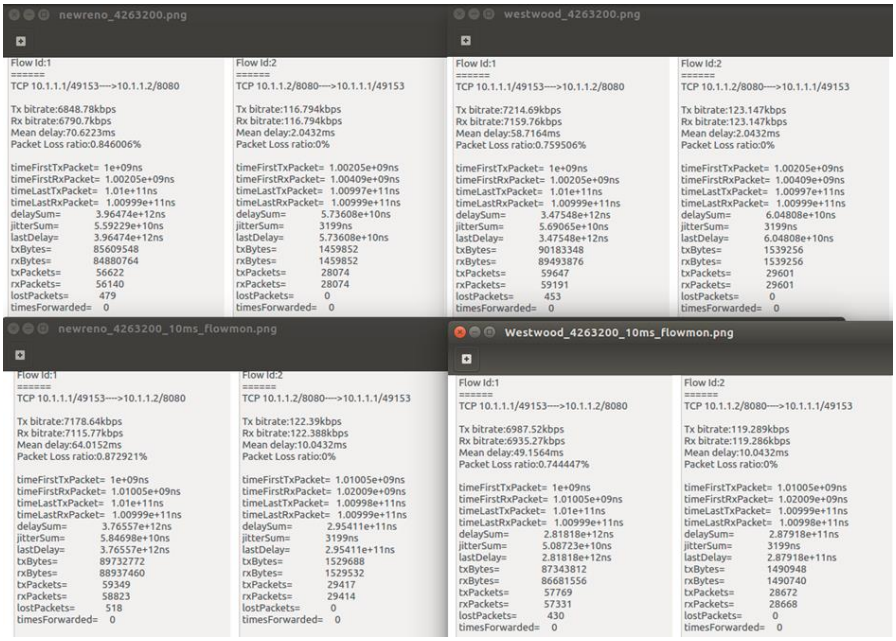

Fig. 4.35 Comparison using a sender buffer size=4263200 Bytes and different delay values and TCP modes. On the top the delay is 2 ms. on the bottom is 10 ms.

With a delay of 10ms and a buffer size of 14600 Bytes (Fig. 4.34), the throughput decreases drastically while the mean delay increases, as expected. Instead, using a buffer size of 4263200 Bytes (Fig. 4.35), the result to highlight is that, despite an increasing in the propagation delay, the mean delay decreases when

using a delay value of 10ms. The reason of this behavior is a re-connection that happens when using a 10 ms, as showed in Fig. 4.36 (for Westwood is the same).

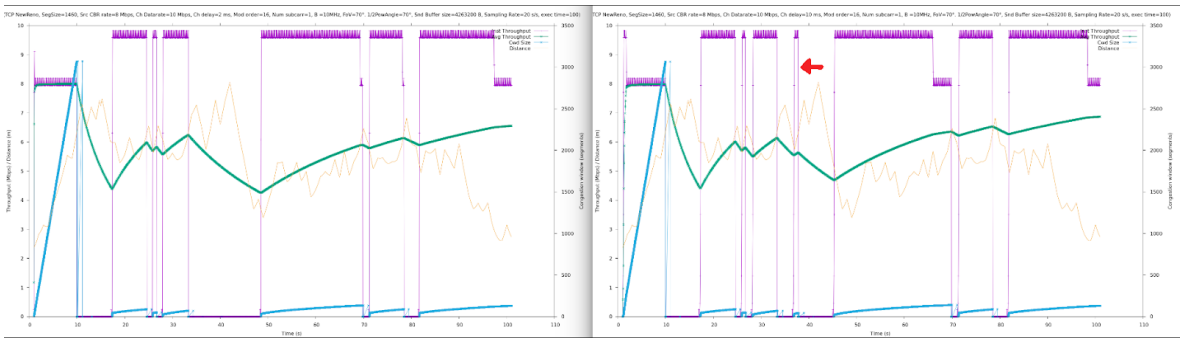

Fig. 4.36 Instantaneous throughput using New Reno, a sender buffer size = 4263200 Bytes and a delay time of 2ms (on the left) and 10ms (on the right)

About the differences between the two TCP modes, New Reno performs better in terms of average Throughput when the delay increases, while Westwood does the opposite. In terms of mean delay, Westwood continues to perform better.

Source application data rate

Two different values for the application source data rate, 8 Mbps and 12 Mbps, and sender buffer sizes, 14600 Bytes and 4263200 Bytes, have been used. It is worth to remember that the source application produces traffic at constant bit rate and the channel delay is set to 2 ms.

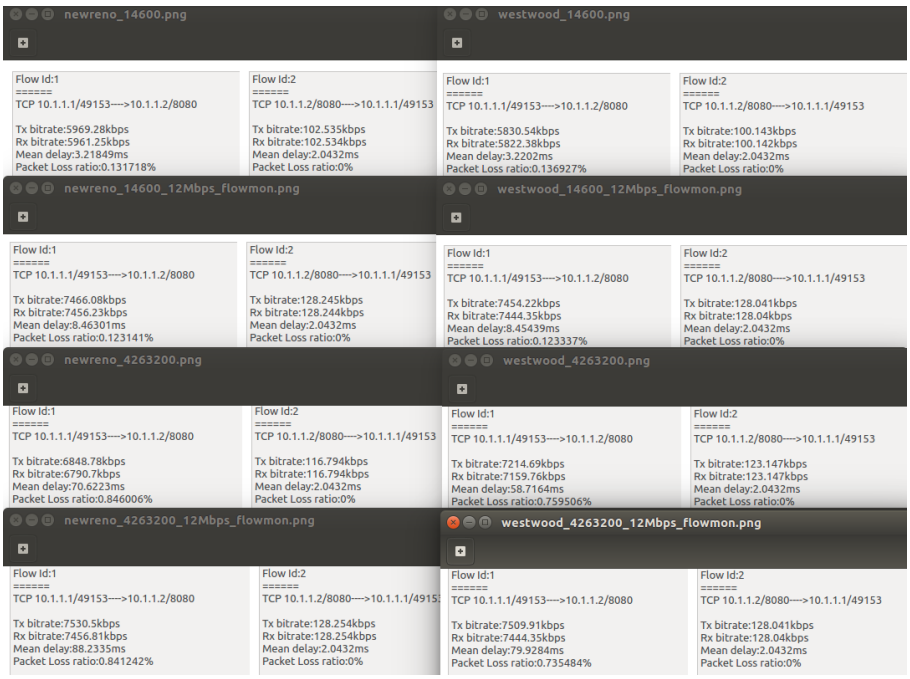

Fig. 4.37 Comparison using different source application data rate (8 Mbps and 12 Mbps), sender buffer sizes (14600 Bytes and 4263200 Bytes) and TCP modes. The parameters used are specified in each picture name.

When using a source data rate of 12 Mbps, the average throughput increases, and it is limited by the channel data rate that is 10 Mbps. However, the value doesn't reach this maximum in the average because, as showed in Fig. 4.30, the receiver is not always in the coverage area. About the mean delay, it increases in all the cases.

A remarkable result is that with this higher source data rate, the difference in the average throughput among the different sender buffer sizes almost disappears, while the difference in the mean delay remain equal.

About the TCP performance, there are no important differences between New Reno and Westwood for the small buffer size. Instead, for the big buffer size, Westwood performs better in terms of mean delay and BER.

4.1.3 Results highlights

In this section are listed some considerations based on the observation of simulation results:

- **Modulation order:** in the considered scenario, it is possible to use high modulation order because the SNR is always higher than 35 dB (Fig. 4.30), when the device is in the coverage area, and it is feasible to use even a 1024 QAM scheme [47].
- **Slow start Threshold:** except for the first interval of connection, this value is different for the two algorithms, since they manage the $ssthresh$ in a different way (TCP New Reno → $ssthresh = CongWin/2$ | TCP Westwood → $ssthresh$ is dynamically adjusted depending on the ACK).
- **Angles:** The FOV angle is the main parameter that affects the PHY channel in this scenario, since we are considering just one transmitter with a high transmitted power and no interfering sources. For this scenario, in order to maximize the coverage area, it is better to have a receiver with a wide FOV angle.
- **Sender Buffer Size:** this parameter is really important because it considerably affects both the throughput and the end-to-end delay. From the simulations, it seems that using a big buffer size (e.g. 4263200 B) is the best solution in almost all the cases.

Finally, about the two analyzed TCP congestion control mechanisms:

As discussed in all the previous subsections, Westwood seems to perform better in almost all the cases analyzed, especially in terms of mean delay and BER.

4.2 LiFi module results

This section aims to validate the developed module, comparing the results obtained using it with the ones presents in [52], one of the reference paper in this field. In addition, the network and transport layers are tested using different scenarios.

4.2.1 Received power and SINR

The scenario is the one described in [52] and already presented in Section 3.4.

Each cell is divided in 19 sub-cells, each one served by a different LED cluster of the LED array Fig. 4.38 a), and they used a small half-power angle (10°) to confine most of the signal power within each sub-cell. Furthermore, it is assigned different sub-bands for the internal and the external region of a cell Fig. 4.38 b).

The SINR for the *j-th* sub-channel is calculated as follows:

$$SINR_j = \frac{\left(\sum_{i=S} \rho H_{i,j,n} P_{i,j}\right)^2}{\left(\sum_{k=I_j} \rho H_{k,j} P_{k,j}\right)^2 + \sigma^2} \quad \textbf{(5.1)}$$

where S is the serving stations, I_j is the interfering stations for sub-channel j, ρ is responsivity of PD, $P_{i,j}$ power of transmitter array i for sub-channel j, $H_{i,j}$ is the channel DC gain (Equation 1.7) between transmitter i and user n, σ^2 is the noise power.

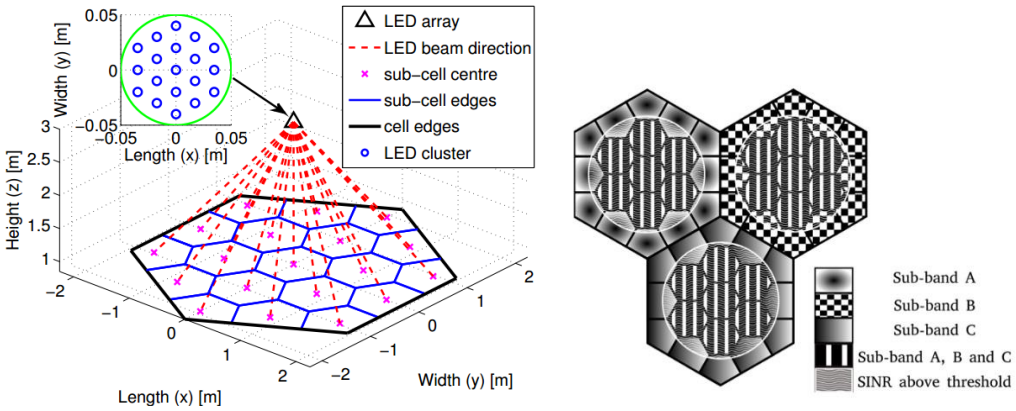

Fig. 4.38 a) On the left, the coverage arrangement in a cell. Each LED cluster in the LED array covers a different region of a cell. b) On the right, deployment of fractional frequency reuse in an optical wireless system [52]

Since this approach would have been too complex to implement (19*13=247 sub-cells), the choice to implement just the 13 main cells using the full frequency reuse approach with 3 different sub-bands.

In addition, single LED bulbs (point light sources), and wide semi-angle half power of 70° have been used, instead of complex LEDs arrays with different beam directions. The parameters used are the ones in **¡Error! No se encuentra el origen de la referencia.**4

Table 4.4 Simulation parameters used for the 2nd scenario

	Parameter	*Value*
Transmitter	Transmitted Power	$32.256\ W$
	Semiangle Half Power	$70°$
Receiver	Photodetector Active Area	$1.5\ cm^2$
	Field of View Angle	$70°$
	Refractive Index	1.5
	Optical Filter Gain	1
	Photodetector Responsivity	$0.28\ A/W$
System	Bandwidth	$20\ MHz$
	Number of Subcarriers	100
	Carrier spacing	$195.32\ kHz$
	Noise Power Spectral Density	$1 \times 10^{-21}\ A^2/Hz$

These are the results of the simulations made with the LiFi module:

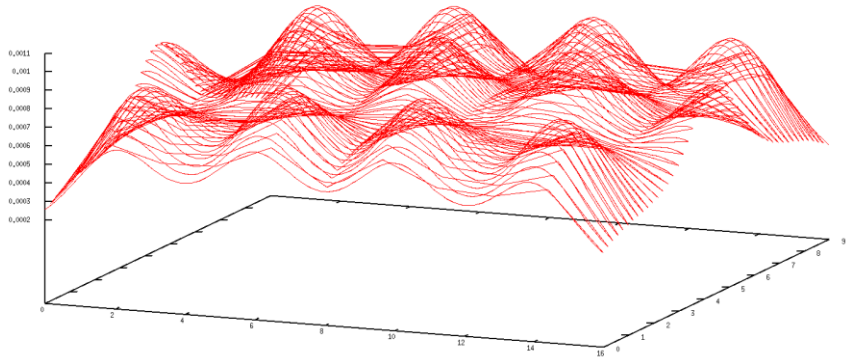

Fig. 4.39 Received signal considering all the bands

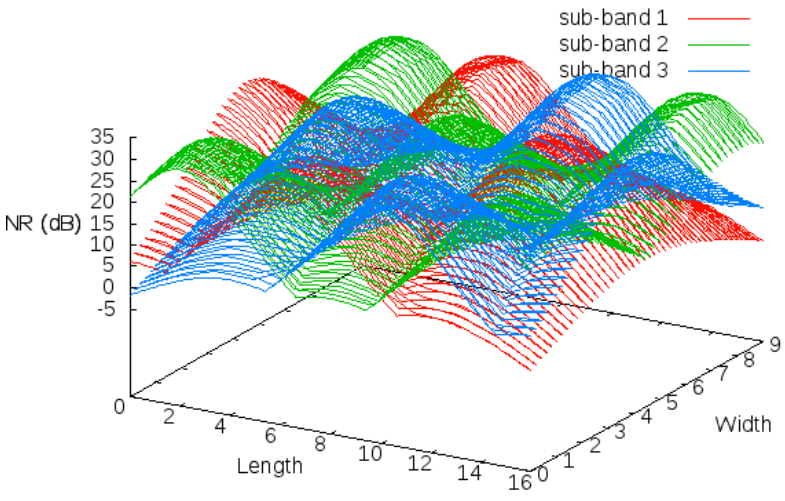

Fig. 4.40 The plot of the SINR value for each sub band

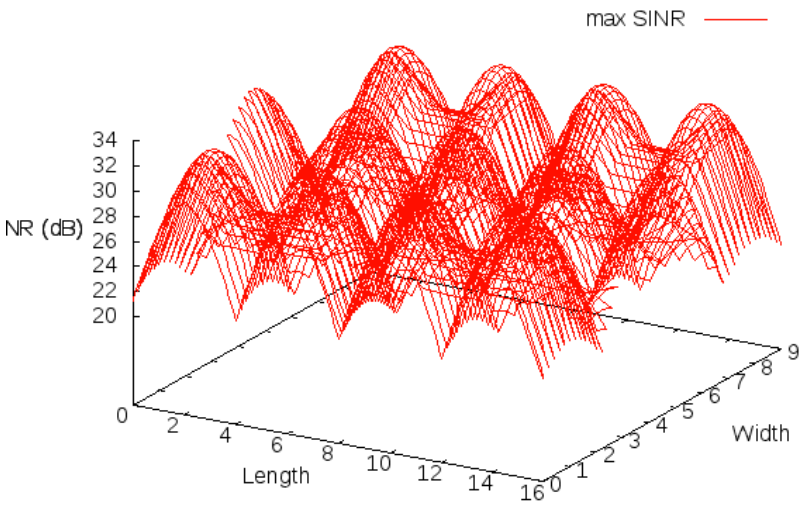

Fig. 4.41 Plot of the SINR distribution over the three sub-bands taking the MAX in each point

Taking into account the "simplification" of the scenario, the results showed match with the one in [52]. Thus, we can consider that the physical layer implemented in LiFi is working properly.

4.2.2 TCP performance

In addition, also the network and transport layer functionalities have been tested with a simple scenario, just one AP and one user, with the topology in Fig. 4.42 and using three different mobility models. In addition, the parameters suggested in the IEEE 802.15.7r1 [53] for OFDM frequency have been used. The results are showed in the Annexes.

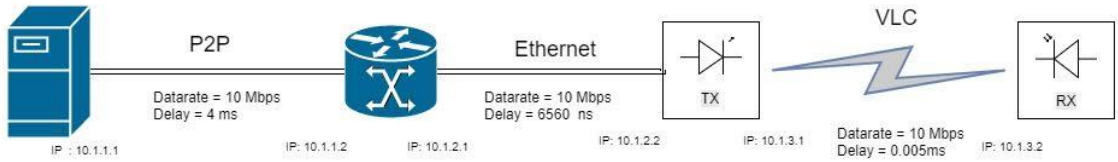

Fig. 4.42 Network topology used to test the network and transport layer functionalities of the LiFi module.

CONCLUSIONS

The current RF technologies will not be able to satisfy the increasing traffic demand due to their intrinsic limitations (mainly the limited bandwidth). This motivated the research to focus on the other parts of the Electromagnetic spectrum, like the optical spectrum. Thanks to the large market adoption of the LEDs, with their fast switching capabilities, as lightening source, the Visible Light Communication technology has emerged as the most promising OWC technology.

Since the low interest that the network and transport layer has captured in the VLC research, this study has focused on these aspects. Thus, the first problem to face has been that all the implementations of the VLC channel are just for simulators that don't handle the network functionalities and no network simulator has an official module for it. For this reason, the first step has been to decide a network simulator and to add the support for the VLC.

Ns-3 has been chosen because it is one of the most used network simulators and it is open source. As written in the work title, the focus is on the Transport Layer. Thus, the module implemented contained a model of the VLC channel that, well integrated with simulation environment, allowed to analyze the TCP performances over this technology. After defining a basic simulation scenario, several simulations have been performed varying both the physical and network layer parameters.

In the considered scenario, the results obtained demonstrated the good qualities of the channel and, that, the main limitations are due to the physical devices parameters like the FOV and the semi-angle at half-power: in facts, when the user moves, the disconnection happens when the access point is out of the Field of View of the user's receiver and not because the channel degradation due to the low received power, or because the noise. This means that under the coverage of the light source, the system is stable but, when it leaves the coverage zone, the system drastically fails, converting it in a very sensitive network. Nevertheless, this phenomenon could be overcome by introducing more light sources in the same area, so the light covers most of the space. This consideration yielded to the design and implementation of another module, which allowed to simulate more complex scenarios with several access points and users, and a more detail management of the spectrum. This module has been built following the ns3 development rules, in order to be included in the platform after it will be enough mature. Finally, some tests and comparison have been conducted to validate it.

About the TCP analysis, several simulations have been carried out with the variation of different parameters, such as the sender buffer size, the channel

delay and the source application data rate. In all the cases, two different congestion control mechanisms have been tested: New Reno and Westwood. From the results obtained, Westwood performed better in almost all the cases analyzed, especially in terms of mean delay and BER.

The development of the LiFi module is at the first steps: even if the physical channel is enough accurate for most of the scenarios, other components like the NetDevice and the other classes belonging to the MAC layer must be further developed. In addition, the release of the new IEEE standard (802.15.7r1) is expected at the end of the 2018. Thus, the development should follow its recommendations. Based on this module, it would be interesting to analyze the behavior of the TCP in horizontal handover scenarios, another major topic with few research works.

At the end, after all the simulation works, it will be really important to implement all these scenarios in the real world, with real electronic devices.

Sustainability considerations

One of the main benefits of using VLC is its energy efficiency, since the electric power that supplies the LEDs is used for the dual purpose of illumination and data communications. In addition, a VLC network will be easy to deploy because in most of the cases it's possible to use the existing illuminating infrastructure with some small modifications.

Regarding the economic point of view, the low cost of the devices (both the transmitters and receivers), plus the reuse of the existing infrastructures, lead to a relatively low cost of the overall system.

Ethical considerations

VLC brings an inherent physical security, since the visible light, because of its nature, cannot pass through opaque objects (e.g. walls). Nevertheless, encryption must be implemented to provide security in all the use cases, like vehicle to vehicle communication or public indoor environments.

VLC will have a good social impact: it will allow people to be connected to Internet via wireless even in places where it is not allowed because of the possible EM interference.

ANNEXES

LiFi module - Constant position model simulation

The receiver doesn't move (It has a fixed position). We are using all the subcarriers.

Parameters

Num. Transmitters	1
Num. Receivers	1
Position Transmitter	(x,y,z) = (0,0,3)
Position Receiver	(x,y,z) = (0,0,0.85)
Simulation time	30 s

	Parameter	**Value**
Transmitter	Transmited Power	32.256 W
	Semiangle Half Power	70°
Receiver	Photodetector Active Area	$1.5\ cm^2$
	Field of View Angle	70°
	Refractive Index	1.5
	Optical Filter Gain	1
	Photodioder Responsivity	0.28 A/W
System	Bandwith	20 MHz
	Number of Subcarriers	100
	Carrier spacing	195.32 kHz
	Noise Power Spectral Density	$1 \times 10^{-21}\ A^2/Hz$

Plots

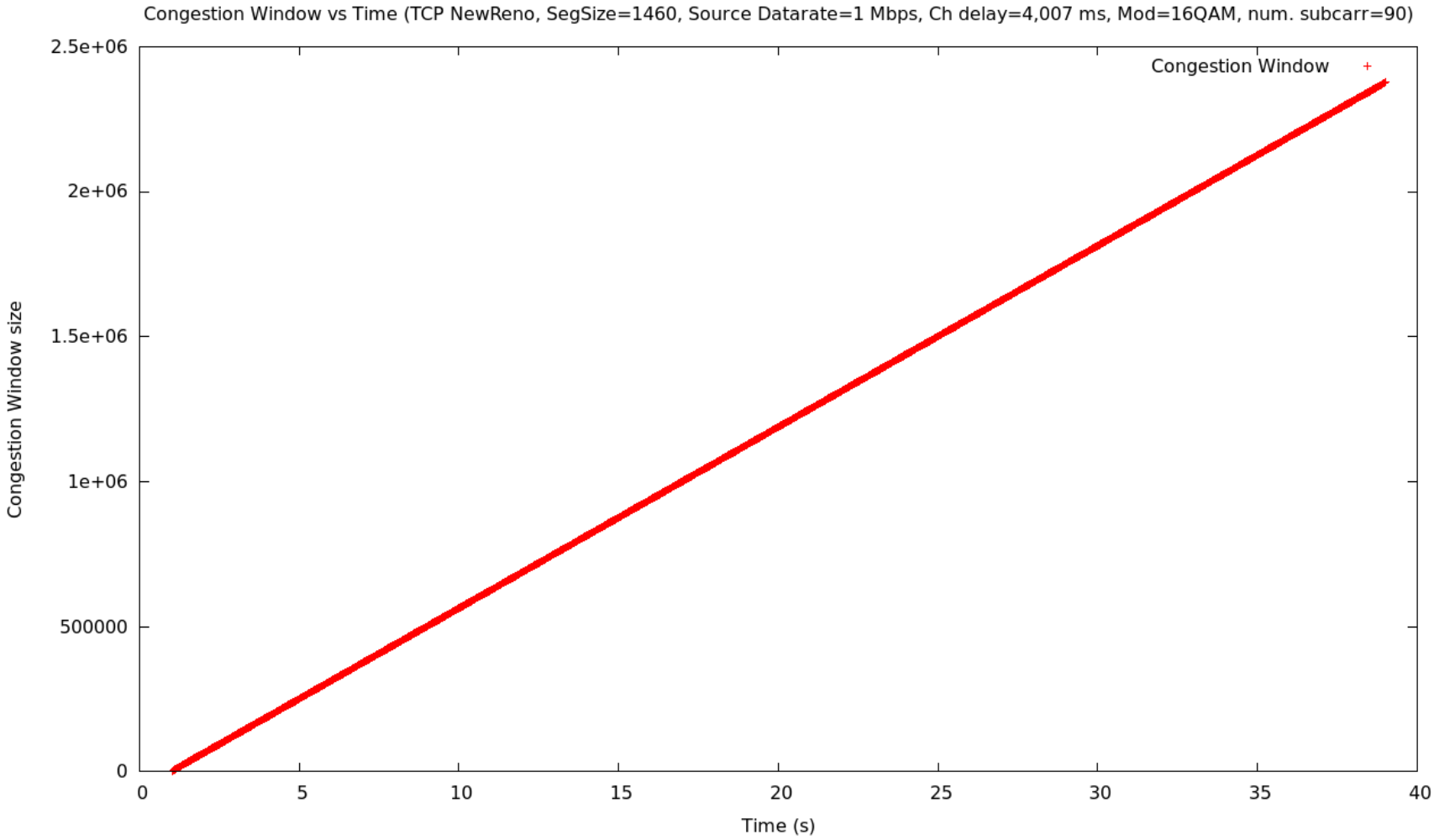
Congestion Window vs Time (TCP NewReno, SegSize=1460, Source Datarate=1 Mbps, Ch delay=4,007 ms, Mod=16QAM, num. subcarr=90)
Congestion Window
Congestion Window size
Time (s)
2.5e+06
2e+06
1.5e+06
1e+06
500000
0
0
5
10
15
20
25
30
35
40

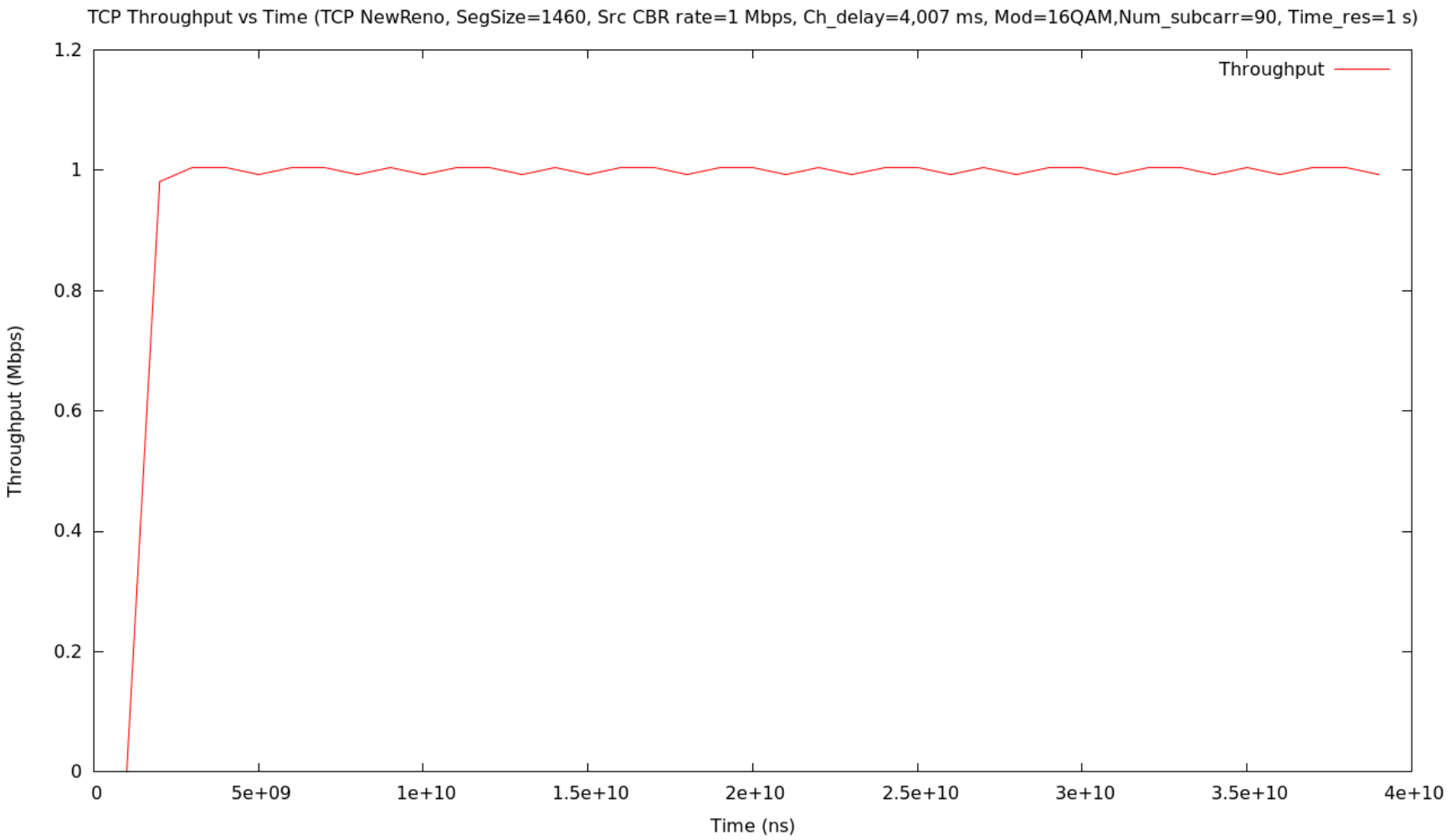
TCP Throughput vs Time (TCP NewReno, SegSize=1460, Src CBR rate=1 Mbps, Ch_delay=4,007 ms, Mod=16QAM,Num_subcarr=90, Time_res=1 s)
Throughput
Throughput (Mbps)
Time (ns)
0
0.2
0.4
0.6
0.8
1
1.2
0
5e+09
1e+10
1.5e+10
2e+10
2.5e+10
3e+10
3.5e+10
4e+10

```
Flow Id:1
======
TCP 10.1.1.1/49153---->10.1.3.2/8080

Tx bitrate:1035.3kbps
Rx bitrate:1035.58kbps
Mean delay:7.67158ms
Packet Loss ratio:0%

timeFirstTxPacket=  1e+09ns
timeFirstRxPacket=  1.01438e+09ns
timeLastTxPacket=  3.90083e+10ns
timeLastRxPacket=  3.90125e+10ns
delaySum=          2.49863e+10ns
jitterSum=         1.97755e+07ns
lastDelay=         2.49863e+10ns
txBytes=           4918748
rxBytes=           4918748
txPackets=         3257
rxPackets=         3257
lostPackets=       0
timesForwarded=    6514

delayHistogram nBins:15
Index:4 Start:0.004 Width:0.001 Count:3
Index:7 Start:0.007 Width:0.001 Count:3252
Index:8 Start:0.008 Width:0.001 Count:1
Index:14 Start:0.014 Width:0.001 Count:1

jitterHistogram nBins:11
Index:0 Start:0 Width:0.001 Count:3251
Index:1 Start:0.001 Width:0.001 Count:2
Index:3 Start:0.003 Width:0.001 Count:2
Index:10 Start:0.01 Width:0.001 Count:1

packetSizeHistogram nBins:76
Index:2 Start:40 Width:20 Count:4
Index:75 Start:1500 Width:20 Count:3253
```

```
Flow Id:2
======
TCP 10.1.3.2/8080---->10.1.1.1/49153

Tx bitrate:17.8389kbps
Rx bitrate:17.8423kbps
Mean delay:4.17279ms
Packet Loss ratio:0%

timeFirstTxPacket=  1.01438e+09ns
timeFirstRxPacket=  1.02576e+09ns
timeLastTxPacket=  3.90042e+10ns
timeLastRxPacket=  3.90083e+10ns
delaySum=          6.79747e+09ns
jitterSum=         7.21392e+06ns
lastDelay=         6.79747e+09ns
txBytes=           84712
rxBytes=           84712
txPackets=         1629
rxPackets=         1629
lostPackets=       0
timesForwarded=    3258

delayHistogram nBins:12
Index:4 Start:0.004 Width:0.001 Count:1628
Index:11 Start:0.011 Width:0.001 Count:1

jitterHistogram nBins:8
Index:0 Start:0 Width:0.001 Count:1627
Index:7 Start:0.007 Width:0.001 Count:1

packetSizeHistogram nBins:3
Index:2 Start:40 Width:20 Count:1629
```

```
Flow Probes:

Index:0
 FlowId:1 Packets:3257 Bytes:4918748 DelayFromFirstProbeSum:0ns
 FlowId:2 Packets:1629 Bytes:84712 DelayFromFirstProbeSum:6.79747e+09ns

Index:1

Index:2
 FlowId:1 Packets:3257 Bytes:4918748 DelayFromFirstProbeSum:1.69695e+10ns
 FlowId:2 Packets:1629 Bytes:84712 DelayFromFirstProbeSum:2.11095e+08ns

Index:3

Index:4
 FlowId:1 Packets:3257 Bytes:4918748 DelayFromFirstProbeSum:2.09789e+10ns
 FlowId:2 Packets:1629 Bytes:84712 DelayFromFirstProbeSum:1.02064e+08ns

Index:5

Index:6
 FlowId:1 Packets:3257 Bytes:4918748 DelayFromFirstProbeSum:2.49863e+10ns
 FlowId:2 Packets:1629 Bytes:84712 DelayFromFirstProbeSum:0ns
```

LiFi module - Constant speed model simulation

The receiver moves with a speed of 0.5 m/s on the x-axis with a positive direction. It starts at point (-1, 0, 0.85). All the subcarriers have been used.

Parameters

Num. Transmitters	1
Num. Receivers	1
Position Transmitter	(x,y,z) = (0,0,3)
Simulation time	30 s

	Parameter	Value
Transmitter	Transmited Power	32.256 W
	Semiangle Half Power	70°
Receiver	Photodetector Active Area	1.5 cm^2
	Field of View Angle	70°
	Refractive Index	1.5
	Optical Filter Gain	1
	Photodioder Responsivity	0.28 A/W
System	Bandwith	20 MHz
	Number of Subcarriers	100
	Carrier spacing	195.32 kHz
	Noise Power Spectral Density	$1 \times 10^{-21}\ A^2/Hz$

Plots

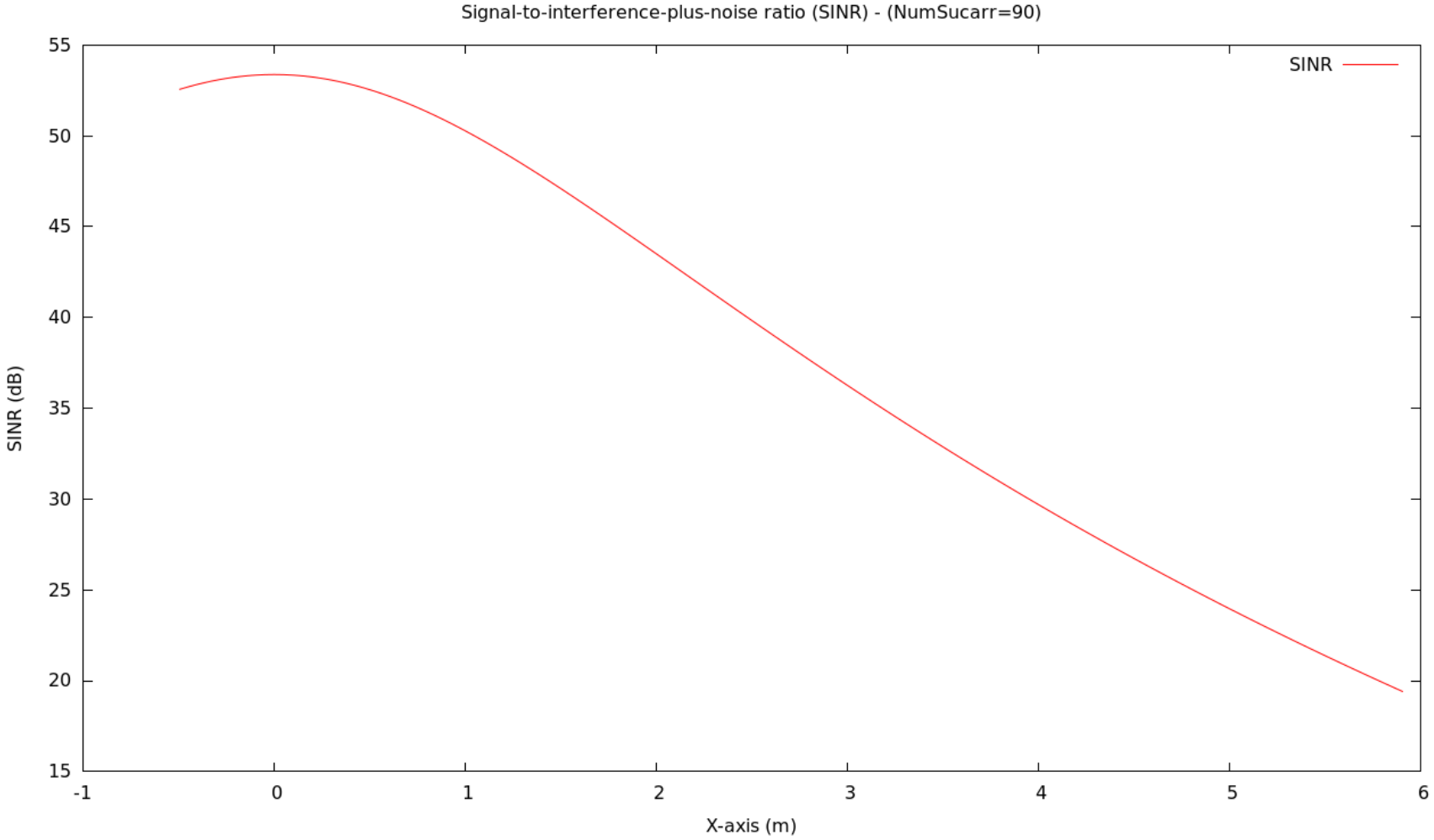
Signal-to-interference-plus-noise ratio (SINR) - (NumSucarr=90)
SINR
SINR (dB)
X-axis (m)
55
50
45
40
35
30
25
20
15
-1
0
1
2
3
4
5
6

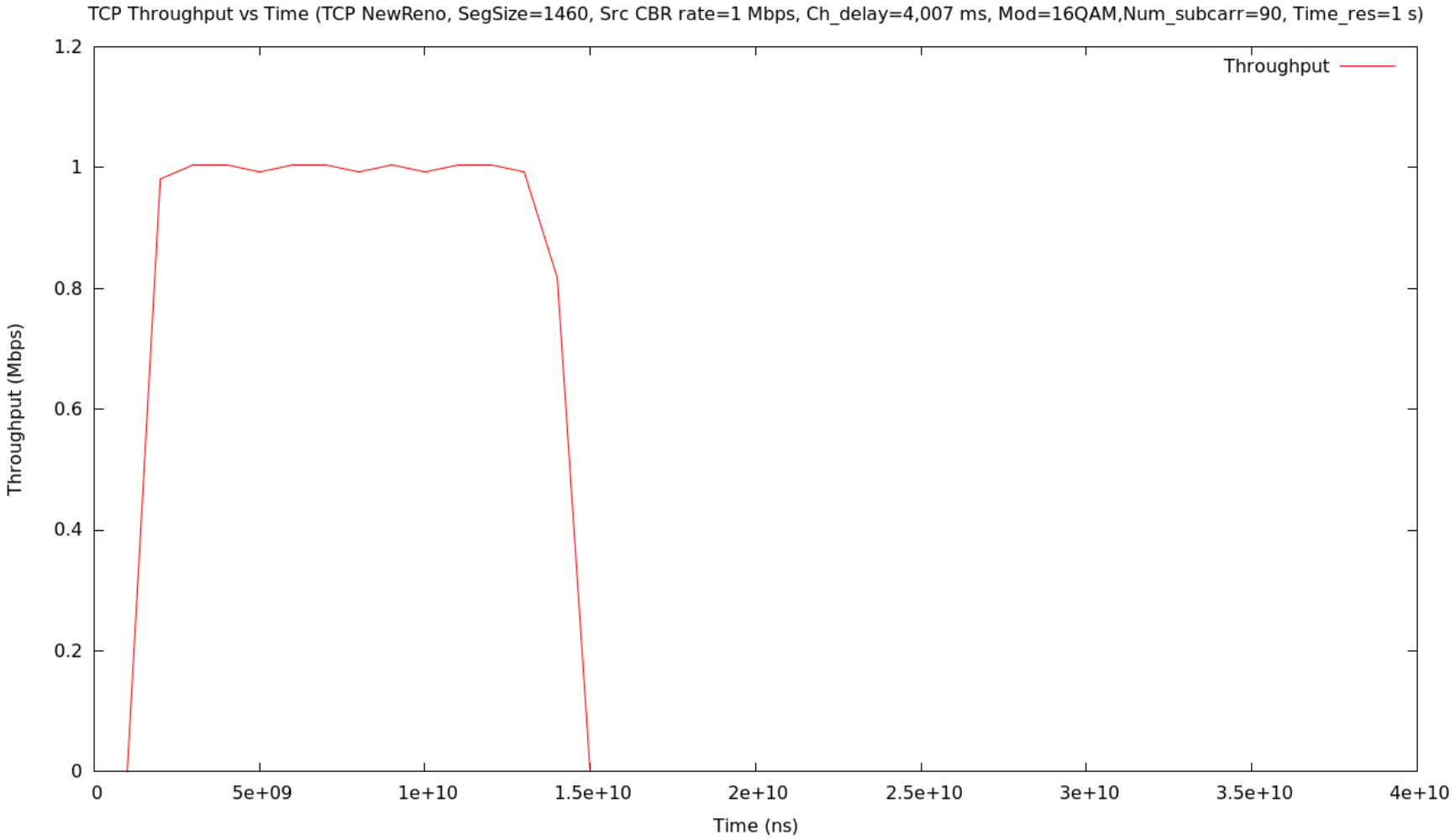
TCP Throughput vs Time (TCP NewReno, SegSize=1460, Src CBR rate=1 Mbps, Ch_delay=4,007 ms, Mod=16QAM,Num_subcarr=90, Time_res=1 s)
Throughput
Throughput (Mbps)
Time (ns)
0
0.2
0.4
0.6
0.8
1
1.2
0
5e+09
1e+10
1.5e+10
2e+10
2.5e+10
3e+10
3.5e+10
4e+10

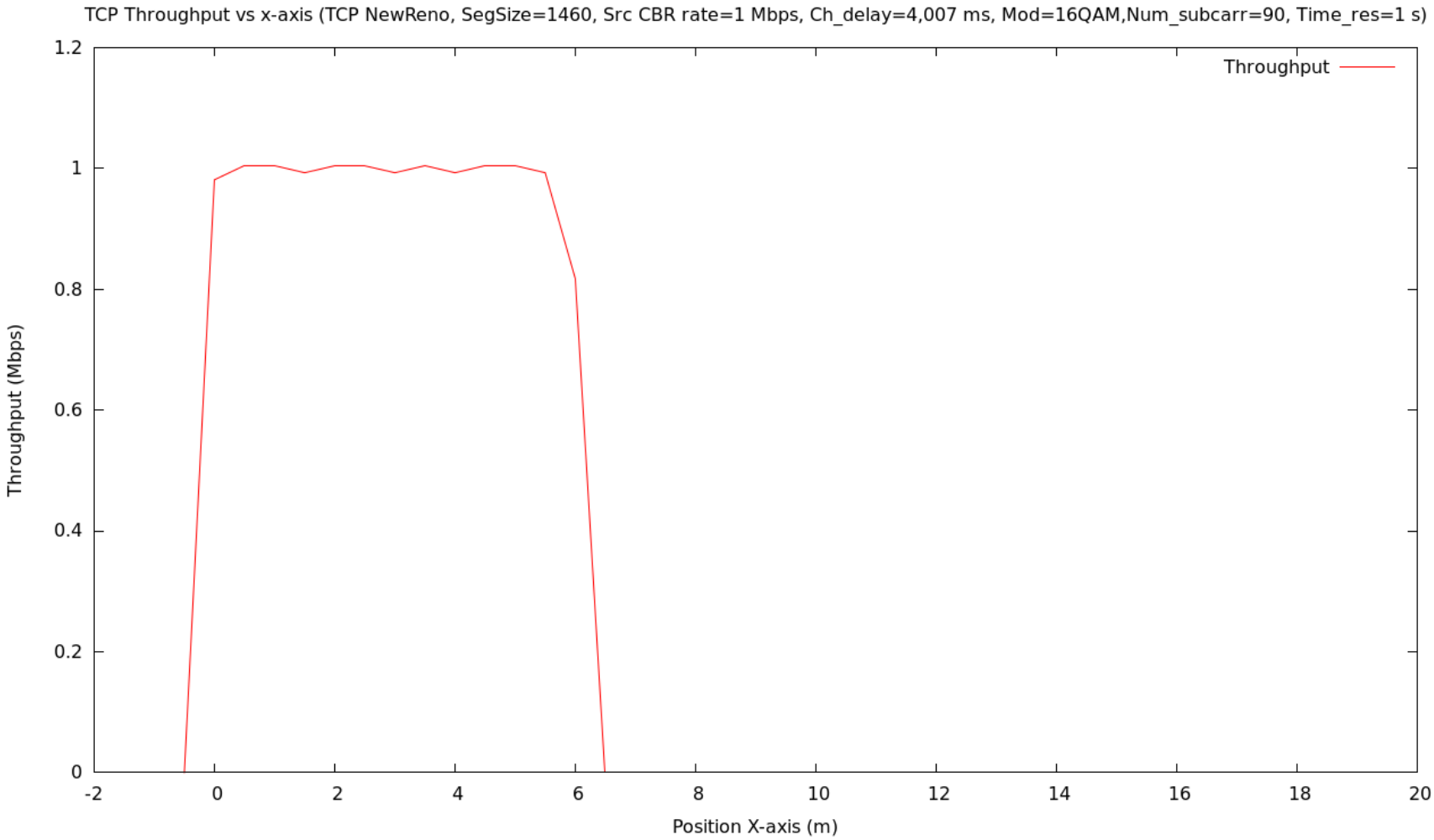
TCP Throughput vs x-axis (TCP NewReno, SegSize=1460, Src CBR rate=1 Mbps, Ch_delay=4,007 ms, Mod=16QAM,Num_subcarr=90, Time_res=1 s)
Throughput
Throughput (Mbps)
Position X-axis (m)
1.2
1
0.8
0.6
0.4
0.2
0
-2
0
2
4
6
8
10
12
14
16
18
20

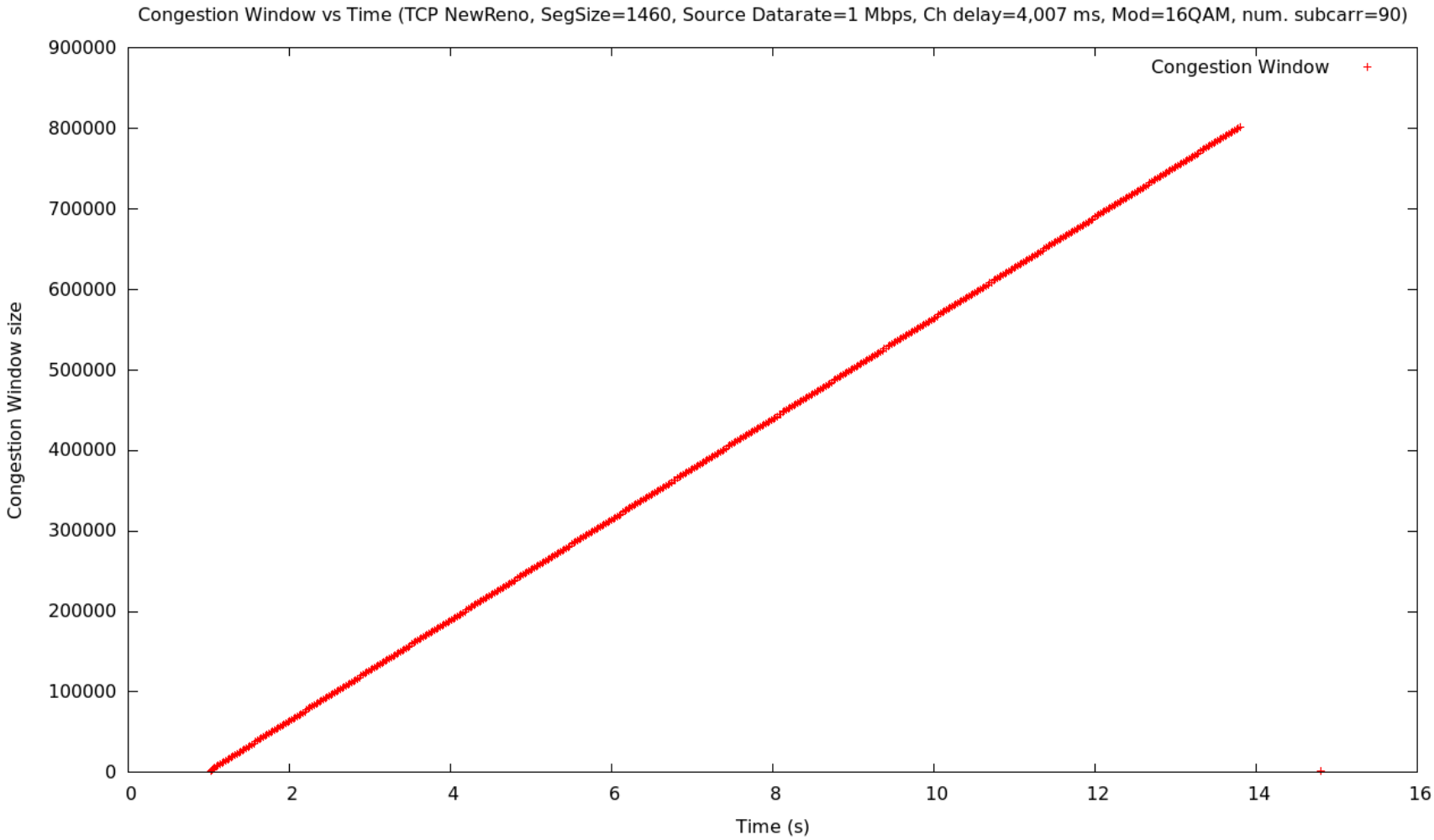
Congestion Window vs Time (TCP NewReno, SegSize=1460, Source Datarate=1 Mbps, Ch delay=4,007 ms, Mod=16QAM, num. subcarr=90)
Congestion Window
Congestion Window size
Time (s)
900000
800000
700000
600000
500000
400000
300000
200000
100000
0
0
2
4
6
8
10
12
14
16

```
Flow Id:1
======
TCP 10.1.1.1/49153---->10.1.3.2/8080

Tx bitrate:1035.3kbps
Rx bitrate:1035.58kbps
Mean delay:7.67158ms
Packet Loss ratio:0%

timeFirstTxPacket=  1e+09ns
timeFirstRxPacket=  1.01438e+09ns
timeLastTxPacket=   3.90083e+10ns
timeLastRxPacket=   3.90125e+10ns
delaySum=           2.49863e+10ns
jitterSum=          1.97755e+07ns
lastDelay=          2.49863e+10ns
txBytes=            4918748
rxBytes=            4918748
txPackets=          3257
rxPackets=          3257
lostPackets=        0
timesForwarded=     6514

delayHistogram nBins:15
Index:4 Start:0.004 Width:0.001 Count:3
Index:7 Start:0.007 Width:0.001 Count:3252
Index:8 Start:0.008 Width:0.001 Count:1
Index:14 Start:0.014 Width:0.001 Count:1

jitterHistogram nBins:11
Index:0 Start:0 Width:0.001 Count:3251
Index:1 Start:0.001 Width:0.001 Count:2
Index:3 Start:0.003 Width:0.001 Count:2
Index:10 Start:0.01 Width:0.001 Count:1

packetSizeHistogram nBins:76
Index:2 Start:40 Width:20 Count:4
Index:75 Start:1500 Width:20 Count:3253
```

```
Flow Id:2
======
TCP 10.1.3.2/8080---->10.1.1.1/49153

Tx bitrate:17.8389kbps
Rx bitrate:17.8423kbps
Mean delay:4.17279ms
Packet Loss ratio:0%

timeFirstTxPacket=  1.01438e+09ns
timeFirstRxPacket=  1.02576e+09ns
timeLastTxPacket=   3.90042e+10ns
timeLastRxPacket=   3.90083e+10ns
delaySum=           6.79747e+09ns
jitterSum=          7.21392e+06ns
lastDelay=          6.79747e+09ns
txBytes=            84712
rxBytes=            84712
txPackets=          1629
rxPackets=          1629
lostPackets=        0
timesForwarded=     3258

delayHistogram nBins:12
Index:4 Start:0.004 Width:0.001 Count:1628
Index:11 Start:0.011 Width:0.001 Count:1

jitterHistogram nBins:8
Index:0 Start:0 Width:0.001 Count:1627
Index:7 Start:0.007 Width:0.001 Count:1

packetSizeHistogram nBins:3
Index:2 Start:40 Width:20 Count:1629
```

```
Flow Probes:

Index:0
 FlowId:1 Packets:3257 Bytes:4918748 DelayFromFirstProbeSum:0ns
 FlowId:2 Packets:1629 Bytes:84712 DelayFromFirstProbeSum:6.79747e+09ns

Index:1

Index:2
 FlowId:1 Packets:3257 Bytes:4918748 DelayFromFirstProbeSum:1.69695e+10ns
 FlowId:2 Packets:1629 Bytes:84712 DelayFromFirstProbeSum:2.11095e+08ns

Index:3

Index:4
 FlowId:1 Packets:3257 Bytes:4918748 DelayFromFirstProbeSum:2.09789e+10ns
 FlowId:2 Packets:1629 Bytes:84712 DelayFromFirstProbeSum:1.02064e+08ns

Index:5

Index:6
 FlowId:1 Packets:3257 Bytes:4918748 DelayFromFirstProbeSum:2.49863e+10ns
 FlowId:2 Packets:1629 Bytes:84712 DelayFromFirstProbeSum:0ns
```

LiFi module - Waypoint-base model simulation

The receiver determines its velocity and position at a given time these vectors:

```
Waypoint (Seconds (0.0), Vector (0.0, 0.0, 0.85)));
Waypoint (Seconds (7.5), Vector (5.0, 0.0, 0.85)));
Waypoint (Seconds (10.0), Vector (10.0, 0.0, 0.85)));
Waypoint (Seconds (12.5), Vector (5.0, 0.0, 0.85)));
Waypoint (Seconds (30), Vector (0.0, 0.0, 0.85)));
```

The application that produces the traffic is not always on (read the source code all the subcarriers have been used.

Parameters

Num. Transmitters	1
Num. Receivers	1
Position Transmitter	(x,y,z) = (0,0,3)
Position Receiver	(x,y,z) = (0,0,0.85)
Simulation time	30 s

	Parameter	Value
Transmitter	Transmited Power	32.256 W
	Semiangle Half Power	70°
Receiver	Photodetector Active Area	1.5 cm^2
	Field of View Angle	70°
	Refractive Index	1.5
	Optical Filter Gain	1
	Photodioder Responsivity	0.28 A/W
System	Bandwith	20 MHz
	Number of Subcarriers	100
	Carrier spacing	195.32 kHz
	Noise Power Spectral Density	$1 \times 10^{-21}\ A^2/Hz$

Plots

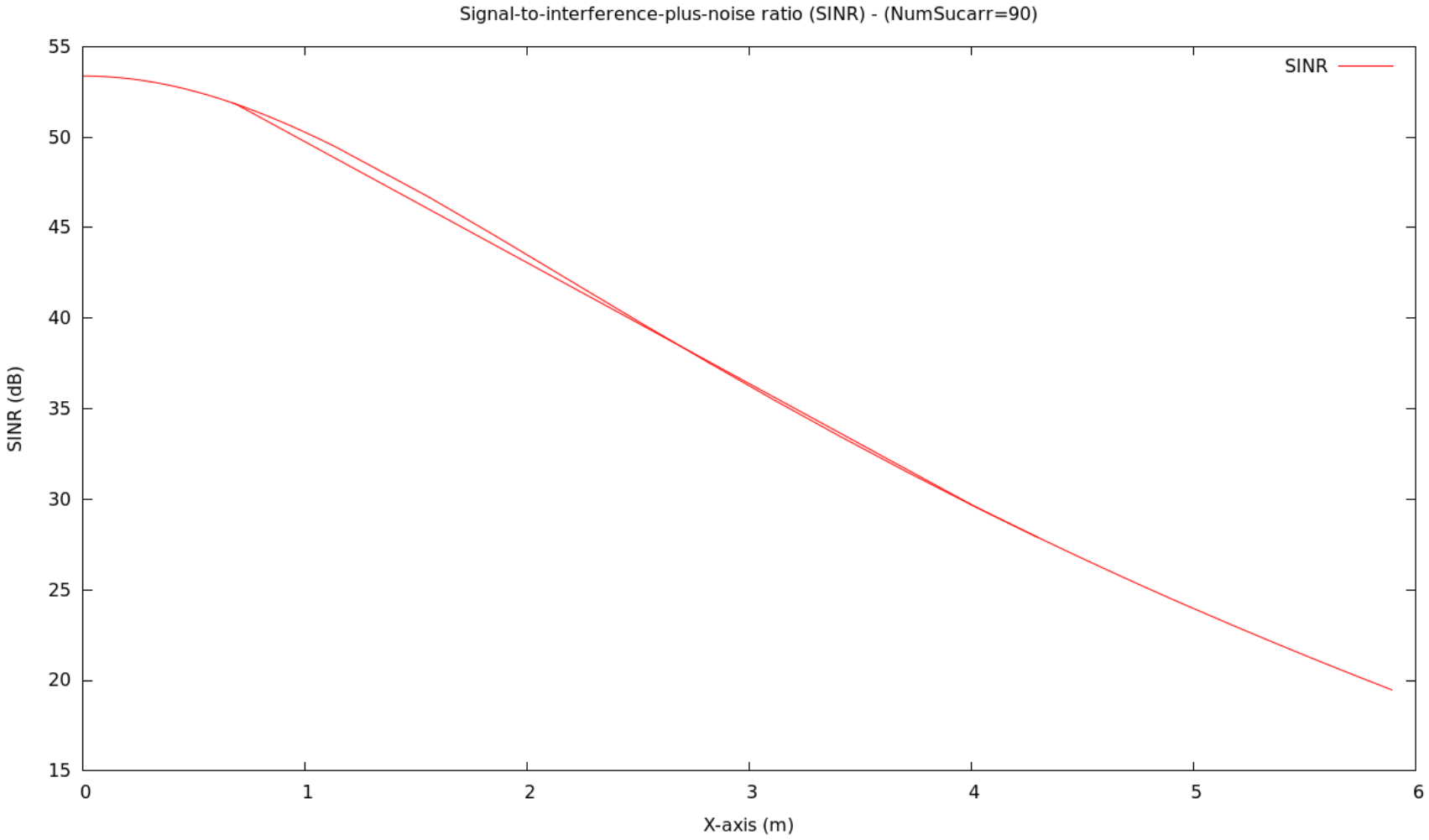
Signal-to-interference-plus-noise ratio (SINR) - (NumSucarr=90)
SINR
SINR (dB)
X-axis (m)
55
50
45
40
35
30
25
20
15
0
1
2
3
4
5
6

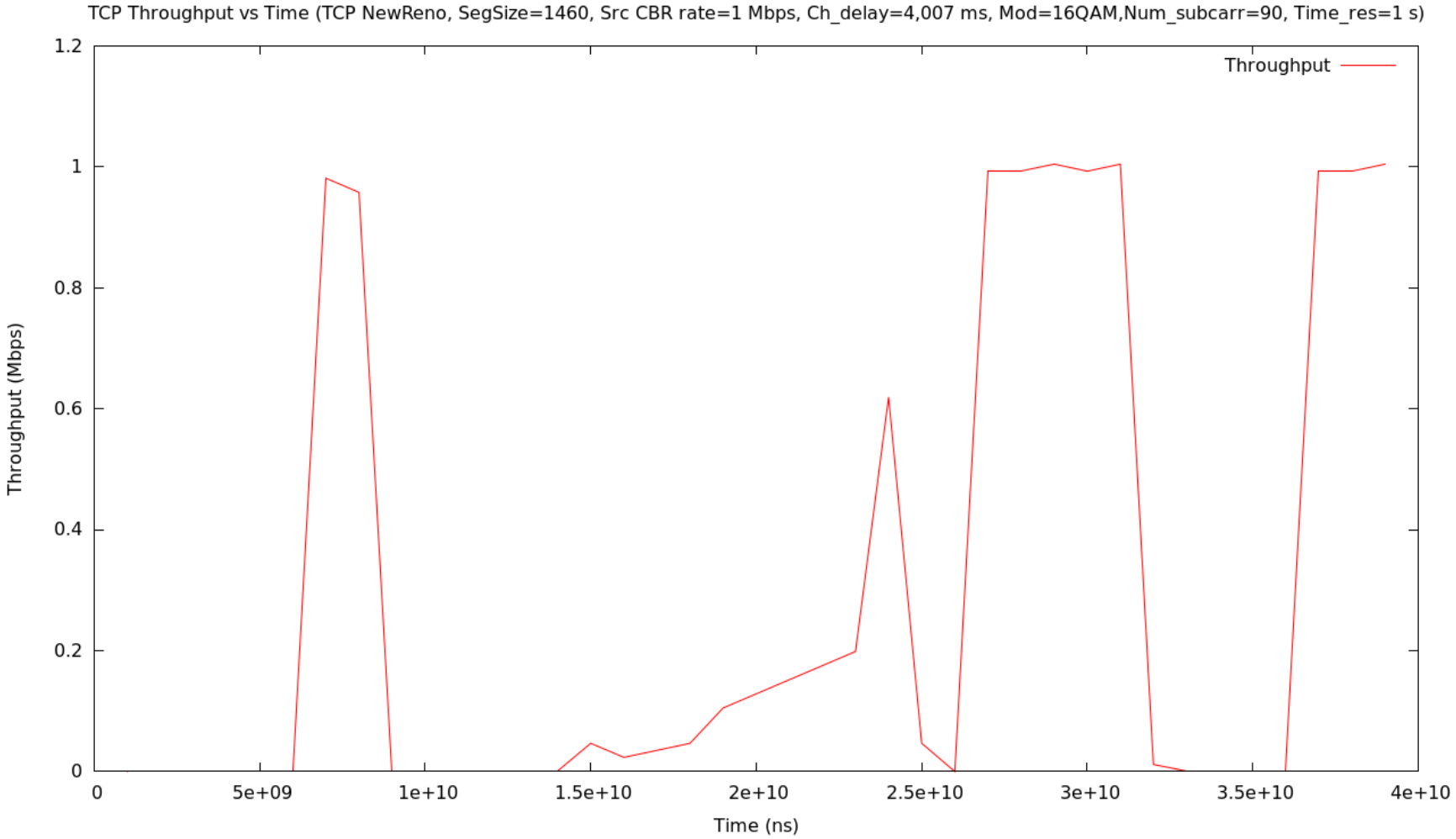
TCP Throughput vs Time (TCP NewReno, SegSize=1460, Src CBR rate=1 Mbps, Ch_delay=4,007 ms, Mod=16QAM,Num_subcarr=90, Time_res=1 s)
Throughput
Throughput (Mbps)
Time (ns)
0
0.2
0.4
0.6
0.8
1
1.2
0
5e+09
1e+10
1.5e+10
2e+10
2.5e+10
3e+10
3.5e+10
4e+10

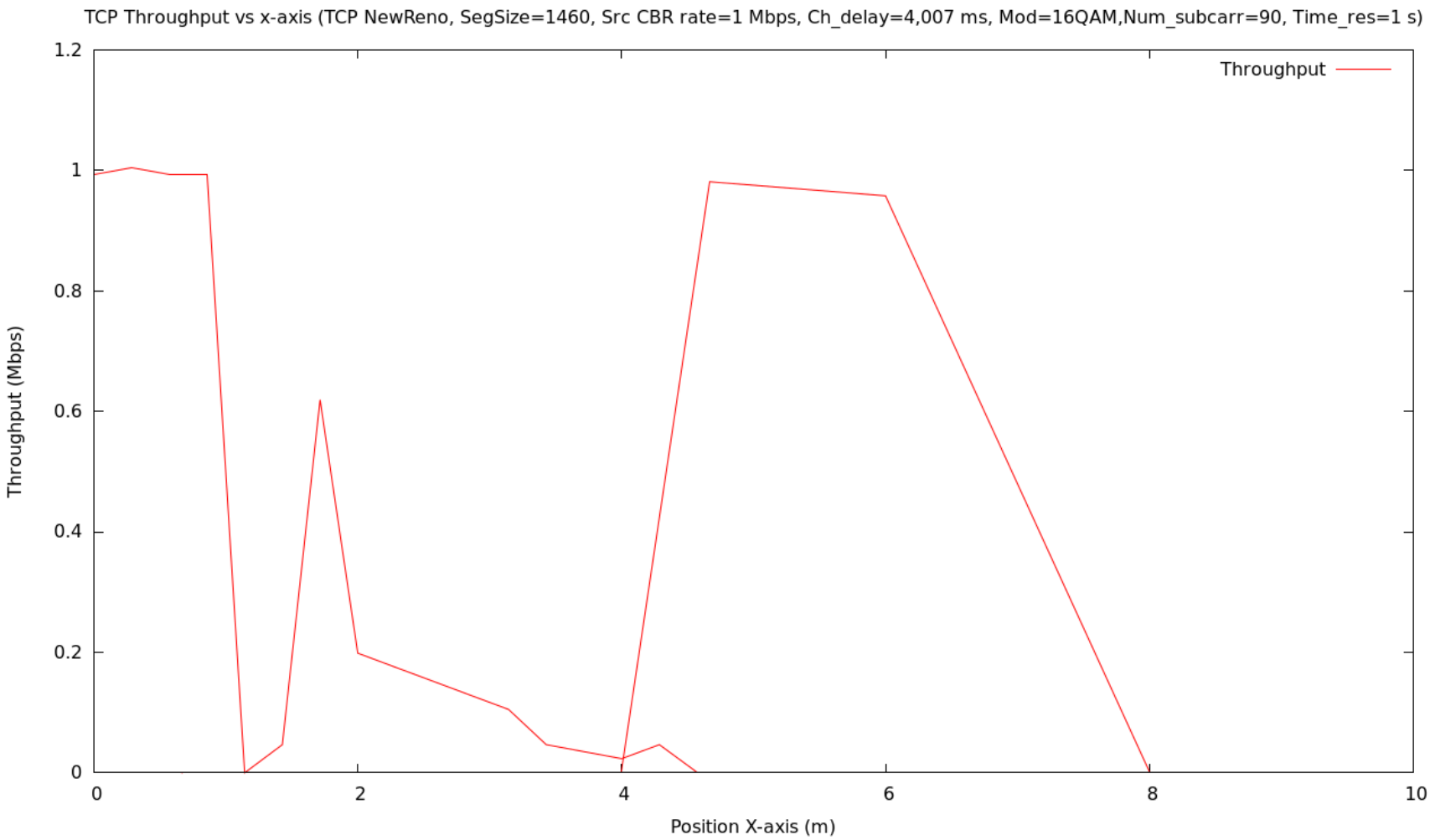
TCP Throughput vs x-axis (TCP NewReno, SegSize=1460, Src CBR rate=1 Mbps, Ch_delay=4,007 ms, Mod=16QAM,Num_subcarr=90, Time_res=1 s)
Throughput
Throughput (Mbps)
Position X-axis (m)
0
0.2
0.4
0.6
0.8
1
1.2
0
2
4
6
8
10

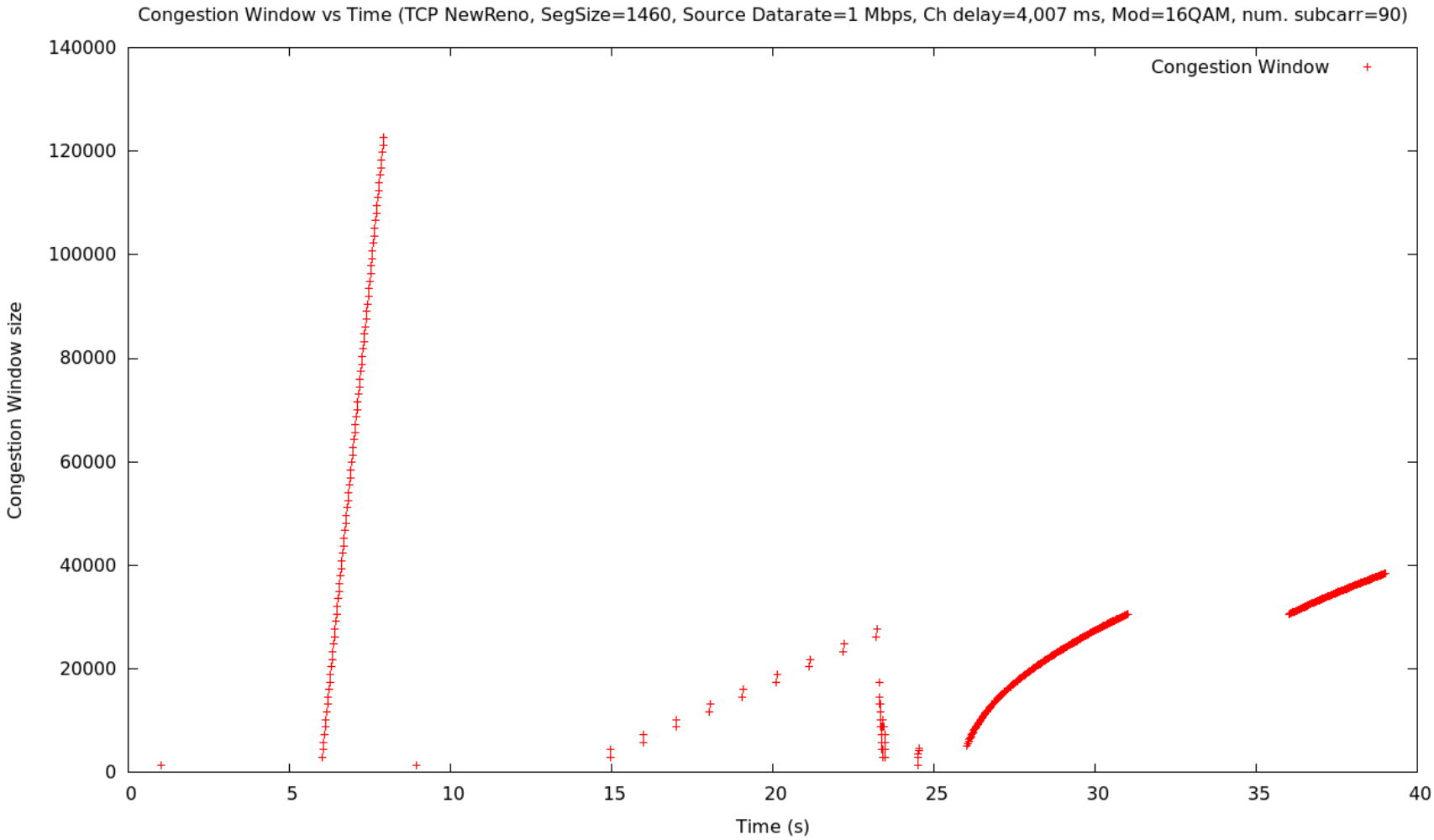
Congestion Window vs Time (TCP NewReno, SegSize=1460, Source Datarate=1 Mbps, Ch delay=4,007 ms, Mod=16QAM, num. subcarr=90)
Congestion Window
Congestion Window size
Time (s)
0
20000
40000
60000
80000
100000
120000
140000
0
5
10
15
20
25
30
35
40

ACRONYMS

5G	fifth Generation
ACO-OFDM	Asymmetrically Clipped Optical OFDM
ADC	Analog-to Digital Converter
AIAD	Additive Increase/Adaptive Decrease
AIMD	Additive Increase/Multiplicative Decrease
BER	Bit Error ratio
CDM	Color Domain Modulations
CP	Cyclic Prefix
DAC	Digital-to Analog Converter
DC	Direct Current
DCO-OFDM	DC-biased Optical OFDM
DSP	Digital Signal Processor
EB	Exabyte
EM	Electromagnetic
FET	Field-Effect-Transistor
FOV	Field-of-View
GPS	Global Position System
IFFT	Inverse Fast Fourier Transform
IM/DD	Intensity Modulation with Direct Detection
IoT	Internet of Things
IP	Internet Protocol
IR	Infrared
ISI	Intersymbol Interference
LEDs	Light-Emitting Diodes
LiFi	Light (Fidelity) Communication Data
LOS	Line-Of-Sight
LTE	Long Term Evolution
MCM	Multi-Carrier Modulations
M-PAM	Module-PAM
M-PSK	M-ary Phase Shift Keying
M-QAM	M-ary Quadrature Amplitude Modulation
M-QAM-N	M-ary QAM OFDM system
MSS	Maximum Segment Size
MTU	Max Transmit Unit
NLOS	Non-Line-Of Sight
NS3	Network Simulator 3
OFDM	Orthogonal Frequency Division Multiplexing
OOK	On-Off Keying
OSI	Open System Interconnection

OWC	Optical Wireless Communication
PAM	Pulse Amplitude Modulation
PAPR	Peak-to-Average Power Ratio
PD	Photodetector
PPM	Pulse Position Modulation
PWM	Pulse Width Modulation
QAM	Quadrature Amplitude Modulation
RF	Radio Frequency (band)
RTT	Round Trip Time
SCM	Single Carrier Modulation
SER	Symbol Error Rate
SNR	Signal-to-Noise-Ratio
TCP	Transmission Control Protocol
TIA	Trance-Impedance Amplifier
UV	Ultraviolet
VLC	Visible Light Communication
VLCP2P	VLC Point-to-Point
VPPM	Variable Pulse Position Modulation
WBANs	Wireless Body Area Networks
Wi-Fi	Wireless (FidelitY) Communication Data
WLAN	Wireless Local Area Network
WPAN	Wireless Personal Area Network

REFERENCES

[1] “5G Vision.” [Online]. Available: https://5g-ppp.eu/wp-content/uploads/2015/02/5G-Vision-Brochure-v1.pdf, Feb. 2015.

[2] S. Wu, H. Wang, and C.-H. Youn, “Visible light communications for 5G wireless networking systems: from fixed to mobile communications,” *IEEE Netw.*, vol. 28, no. 6, pp. 41–45, Nov. 2014.

[3] D. Tsonev, S. Videv, and H. Haas, “Towards a 100 Gb/s visible light wireless access network,” *Opt. Express*, vol. 23, no. 2, p. 1627, Jan. 2015.

[4] P. H. Pathak, X. Feng, P. Hu, and P. Mohapatra, “Visible Light Communication, Networking, and Sensing: A Survey, Potential and Challenges,” *IEEE Commun. Surv. Tutorials*, vol. 17, no. 4, pp. 2047–2077, 2015.

[5] “ns-3.” [Online]. Available: https://www.nsnam.org/.

[6] “Mobile data traffic growth outlook – Ericsson.” [Online]. Available: https://www.ericsson.com/en/mobility-report/reports/november-2017/mobile-data-traffic-growth-outlook.

[7] J. G. Andrews *et al.*, “What Will 5G Be?,” *IEEE J. Sel. Areas Commun.*, vol. 32, no. 6, pp. 1065–1082, June 2014.

[8] S. Arnon, J. Barry, G. Karagiannidis, R. Schober, and M. Uysal, *Advanced Optical Wireless Communication Systems.* Cambridge University Press, 2012.

[9] A. Jovicic, J. Li, and T. Richardson, “Visible light communication: Opportunities, challenges and the path to market,” *IEEE Commun. Mag.*, vol. 51, no. 12, pp. 26–32, 2013.

[10] V. W. S. Wong, R. Schober, D. W. K. Ng, and L.-C. Wang, Eds., *Key Technologies for 5G Wireless Systems*. Cambridge: Cambridge University Press, 2017.

[11] “How much electricity is used for lighting in the United States? - FAQ - U.S. Energy Information Administration (EIA).” [Online]. Available: https://www.eia.gov/tools/faqs/faq.php?id=99&t=3, Feb. 2018.

[12] “Harald Haas: Wireless data from every light bulb | TED Talk.” [Online]. TED Global 2011. Available: https://www.ted.com/talks/harald_haas_wireless_data_from_every_light_bulb.

[13] Cheng Chen, D. Tsonev, and H. Haas, “Joint transmission in indoor visible light communication downlink cellular networks,” in *2013 IEEE Globecom Workshops (GC Wkshps)*, 2013, pp. 1127–1132.

[14] S. Dimitrov and H. Haas, *Principles of LED light communications : towards networked Li-Fi,* Cambridge University Press; 1st ed., 2015.

[15] J. R. Barry, “Wireless Infrared Communications,” vol. 9219, no. 97, 1994.

[16] Z. Ghassemlooy, W. Popoola, and S. Rajbhandari, *Optical Wireless Communications System and Channel Modelling With Matlab.* CRC Pr I Llc, 2017.

[17] A. M. Street, D. C. O'Brien, P. N. Stavrinou, and D. J. Edwards, "Indoor optical wireless systems–a review," *Opt. Quantum Electron.*, vol. 29, no. 3, pp. 349–378, 1997.

[18] U. R. S. Bapst, "Wireless In-House Data Communication via Diffuse Infrared Radiation," *Proc. of the IEEE*, vol. 67, no. 11, 1979.

[19] T. Komine and M. Nakagawa, "Fundamental analysis for visible-light communication system using LED lights," *IEEE Trans. Consum. Electron.*, vol. 50, no. 1, pp. 100–107, 2004.

[20] D. Tsonev, S. Videv, and H. Haas, "Light fidelity ({Li-Fi}): towards all-optical networking," *Proc. SPIE*, vol. 9007, no. 0, pp. 900702–900710, 2013.

[21] A. Žukauskas, M. Shur, and R. Gaska, *Introduction to solid-state lighting*. J. Wiley, 2002.

[22] D. L. DiLaura and Illuminating Engineering Society of North America, *The lighting handbook : reference and application*, 2011.

[23] S. M. Berman, D. S. Greenhouse, I. L. Bailey, R. D. Clear, and T. W. Raasch, "Human electroretinogram responses to video displays, fluorescent lighting, and other high frequency sources.," *Optom. Vis. Sci.*, vol. 68, no. 8, pp. 645–62, Aug. 1991.

[24] I. Standard and I. C. Society, *IEEE Standard for Local and metropolitan area networks — Part 15 . 4 : Low-Rate Wireless Personal Area Networks (LR-WPANs) IEEE Computer Society S ponsored by the*, vol. 2011, no. Sep. 2011.

[25] M. S. Islim and H. Haas, "Modulation Techniques for Li-Fi," @BULLETFi pp. 1673-5188, no. 2, 2016.

[26] A. Aldalbahi *et al.*, "Extending ns3 to simulate visible light communication at network-level," *23rd Int. Conf. Telecommun. ICT 2016*, pp. 2–7, 2016.

[27] J. Vucic and D. Langer, "High-Speed Visible Light Communications: State-of-the-art," *Optical Fiber Communication Conference and Exposition (OFC/NFOEC), 2012 and the National Fiber Optic Engineers Conference*, 4-8 March 2012.

[28] M. Z. Afgani, H. Haas, H. Elgala, and D. Knipp, "Visible Light Communication Using OFDM," *2nd Int. Conf. Testbeds Res. Infrastructures Dev. Networks Communities, 2006. TRIDENTCOM 2006.*, pp. 129–134, 2006.

[29] J. Armstrong and A. J. Lowery, "Power efficient optical OFDM," *Electron. Lett.*, vol. 42, no. 6, p. 370, 2006.

[30] H. Elgala, R. Mesleh, H. Haas, and B. Pricope, "OFDM Visible Light Wireless Communication Based on White LEDs," in *2007 IEEE 65th Vehicular Technology Conference - VTC2007-Spring*, 2007, pp. 2185–2189.

[31] R. Mesleh, H. Elgala, and H. Haas, "Performance analysis of indoor OFDM optical wireless communication systems," in *2012 IEEE Wireless Communications and Networking Conference (WCNC)*, 2012, pp. 1005–1010.

[32] H. Burchardt, N. Serafimovski, D. Tsonev, S. Videv, and H. Haas, "VISIBLE LIGHT COMMUNICATIONS VLC : Beyond Point-to-Point Communication," *Int. J. Adv. Eng. Technol.*, vol. 8, no. July, pp. 98–105, 2014.

[33] H. Elgala, R. Mesleh, and H. Haas, "A study of LED nonlinearity effects on

optical wireless transmission using OFDM," in *2009 IFIP International Conference on Wireless and Optical Communications Networks*, 2009, pp. 1–5.

[34] H. Elgala, R. Mesleh, and H. Haas, "Practical Considerations for Indoor Wireless Optical System Implementation using OFDM," *Contel 2009 Proc. 10th Int. Conf. Telecommun.*, pp. 25–29, 2009.

[35] Z. Wang, C. Yu, W.-D. Zhong, J. Chen, and W. Chen, "Performance of variable M-QAM OFDM visible light communication system with dimming control," in *2012 17th Opto-Electronics and Communications Conference*, 2012, pp. 741–742.

[36] D. Tsonev *et al.*, "A 3-Gb/s Single-LED OFDM-Based Wireless VLC Link Using a Gallium Nitride μLED" *IEEE Photonics Technol. Lett.*, vol. 26, no. 7, pp. 637–640, 2014.

[37] J. van Wyk and L. Linde, "Bit error probability for a M-ary QAM OFDM-based system," in *AFRICON 2007*, 2007, pp. 1–5.

[38] Hao Ma, L. Lampe, and S. Hranilovic, "Integration of indoor visible light and power line communication systems," in *2013 IEEE 17th International Symposium on Power Line Communications and Its Applications*, 2013, pp. 291–296.

[39] S. Shao *et al.*, "An Indoor Hybrid WiFi-VLC Internet Access System," in *2014 IEEE 11th International Conference on Mobile Ad Hoc and Sensor Systems*, 2014, pp. 569–574.

[40] M. B. Rahaim, A. M. Vegni, and T. D. C. Little, "A hybrid Radio Frequency and broadcast Visible Light Communication system," in *2011 IEEE GLOBECOM Workshops (GC Wkshps)*, 2011, pp. 792–796.

[41] J. Zhang, X. Zhang, and G. Wu, "Dancing with light: Predictive in-frame rate selection for visible light networks," in *2015 IEEE Conference on Computer Communications (INFOCOM)*, 2015, pp. 2434–2442.

[42] J. F. Kurose and K. W. Ross, *Computer Networking A Top-Down Approach*, no. 5, 2013.

[43] W.R. Stevens, "TCP Slow Start, Congestion Avoidance, Fast Retransmit, and Fast Recovery Algorithms," RFC 2001, Cat: Standards Track, January 1997.

[44] M. Gerla, M. Y. Sanadidi, Ren Wang, A. Zanella, C. Casetti, and S. Mascolo, "TCP Westwood: congestion window control using bandwidth estimation," in *GLOBECOM'01. IEEE Global Telecommunications Conference (Cat. No.01CH37270)*, vol. 3, pp. 1698–1702.

[45] S. Mascolo *et al.*, "TCP Westwood: Bandwidth Estimation for Enhanced Transport over Wireless Links," *Proc. of the 7th annual international conference on Mobile computing and networking*, Jan. 2001.

[46] J. Mittag, S. Papanastasiou, H. Hartenstein, and E. G. Ström, "Enabling Accurate Cross-Layer PHY / MAC / NET Simulation Studies of Vehicular Communication Networks," *Proc. IEEE*, vol. 99, no. 7, pp. 1311–1326, 2011.

[47] G. S. Navisoy Enriquez, "Analysis of TCP over visible light communication networks," TFM MASTEAM, EETAC. Jul. 2017.

[48] "What is ns-3?" [Online]. Available: https://www.nsnam.org/overview/what-is-ns-3/.

[49] G. F. Riley and T. R. Henderson, “The ns-3 Network Simulator,” in *Modeling and Tools for Network Simulation*, Berlin, Heidelberg: Springer Berlin Heidelberg, 2010, pp. 15–34.

[50] M. Uysal, F. Miramirkhani, O. Narmanlioglu, T. Baykas, and E. Panayirci, “IEEE 802 . 15 . 7r1 Reference Channel Models for Visible Light Communications,” *IEEE Commun. Mag.*, no. January, pp. 212–217, 2017.

[51] N. Baldo and M. Miozzo, “Spectrum-aware Channel and PHY layer modeling for ns3,” *Proc. 4th Int. ICST Conf. Perform. Eval. Methodol. Tools*, no. June 2017, 2009.

[52] Cheng Chen, N. Serafimovski, and H. Haas, “Fractional frequency reuse in optical wireless cellular networks,” *2013 IEEE 24th Annu. Int. Symp. Pers. Indoor, Mob. Radio Commun.*, pp. 3594–3598, 2013.

[53] V. Jungnickel, “Optical Wireless in Beyond 5G,” *Tyrrhenian Workshop on Digital Communicatons*, Sept. 12, 2016, Livorno, Italy.